Single cell dynamics of embryonic muscle progenitor cells in zebrafish

Priyanka Sharma[1], Tyler D. Ruel[1], Katrinka M. Kocha[1], Shan Liao[2], and Peng Huang[1]*

[1]Department of Biochemistry and Molecular Biology, Cumming School of Medicine, Alberta Children's Hospital Research Institute, University of Calgary, 3330 Hospital Drive, Calgary AB T2N 4N1, Canada

[2]Inflammation Research Network, The Snyder Institute for Chronic Diseases, Department of Microbiology, Immunology and Infectious diseases, Cumming School of Medicine, University of Calgary, 3330 Hospital Drive, Calgary AB T2N 4N1, Canada

*Correspondence should be addressed to P.H.

Email: huangp@ucalgary.ca

Tel: 403-220-4612

Running title:

Single cell dynamics of dermomyotome

Keywords:

Dermomyotome, Somite, Muscle progenitor cells, *In vivo* imaging, Extracellular matrix, Zebrafish

Summary statement:

Live imaging and single cell clonal analysis reveal dynamic behaviors of zebrafish embryonic muscle progenitor cells in quiescence and activation.

ABSTRACT

Muscle stem cells hold a great therapeutic potential in regenerating damaged muscles. However, the *in vivo* behavior of muscle stem cells during muscle growth and regeneration is still poorly understood. Using zebrafish as a model, we describe the *in vivo* dynamics and function of dermomyotome cells, a population of embryonic muscle progenitor cells. Dermomyotome cells are located in a superficial layer external to muscle fibers and express many extracellular matrix (ECM) genes including *col1a2*. Utilizing a new *col1a2* transgenic line, we show that dermomyotome cells display a ramified morphology with dynamic cellular processes. Cell lineage tracing demonstrates that *col1a2*$^{+}$ dermomyotome cells contribute to normal muscle growth as well as muscle injury repair. Combination of live imaging and single cell clonal analysis reveals a highly-choreographed process of muscle regeneration. Activated dermomyotome cells change from the quiescent ramified morphology to a polarized and elongated morphology and generate daughter cells that fuse with existing muscle fibers. Ablation of the dermomyotome severely compromises muscle injury repair. Our work provides a dynamic view of embryonic muscle progenitor cells during zebrafish muscle regeneration.

INTRODUCTION

Tissue-resident stem cells are crucial for proper organ development and tissue homeostasis. Skeletal muscles possess remarkable ability to regenerate. To harness the power of stem cells for treatment of diseases such as muscular dystrophy, it is critical to understand how muscle progenitor cells behave *in vivo*. In vertebrates, skeletal muscles originate from the somites (Saga and Takeda, 2001). As the embryo develops, the ventral somite forms the sclerotome, generating progenitors of the axial skeleton and tendons, whereas the dorsolateral somite forms the dermomyotome. The dermomyotome further splits to form the dermatome and the myotome, which contribute to the formation of the skin and skeletal muscles, respectively (Christ and Scaal, 2008; Scaal and Christ, 2004). Thus, the dermomyotome contains embryonic muscle progenitor cells required for the initial formation and growth of the musculature. Fate mapping and lineage tracing experiments in mouse and chick have demonstrated that the dermomyotome is also the source of adult muscle stem cells known as satellite cells (Gros et al., 2005; Kassar-Duchossoy et al., 2005; Relaix et al., 2005; Schienda et al., 2006).

Both the dermomyotome (embryonic muscle progenitor cells) and satellite cells (adult muscle stem cells) contribute to muscle fiber formation, and are marked by the expression of the paired box transcription factors *Pax3* and *Pax7* (Dumont et al., 2015; Scaal and Christ, 2004). However, the function and dynamics of satellite cells have been more extensively studied than those of the dermomyotome. Quiescent satellite cells often display a bipolar morphology and reside beneath the basal lamina on the surface of the muscle fiber (Scharner and Zammit, 2011; Webster et al., 2016). The extracellular matrix (ECM) surrounding the satellite cell constitutes its niche and has been implicated in the regulation of satellite cell behavior (Baghdadi et al., 2018; Bentzinger et al., 2013b; Fry et al., 2017; Rayagiri et al., 2018; Tierney et al., 2016; Urciuolo et al., 2013). In the event of muscle injury, “activated” satellite cells undergo proliferation and initiate the myogenic program. The sequential expression of myogenic regulatory factors, including *Myf5*, *MyoD*, and *Myogenin*, results in the differentiation of myoblasts that align and form new syncytial muscle fibers or fuse with existing myofibers. A single transplanted satellite cell is capable of self-renewal and contribute to muscle fibers (Sacco et al., 2008). Conversely, genetic ablation of satellite cells

in adult mice completely abolishes injury-induced muscle regeneration (Lepper et al., 2011; Murphy et al., 2011; Sambasivan et al., 2011), demonstrating a critical role of satellite cells in maintaining muscle homeostasis.

It has been challenging to visualize the *in vivo* behavior of satellite cells. Previous work has been mostly inferred from "snapshots" of histological sections or analysis from *in vitro* cultures (Bentzinger et al., 2014; El Fahime et al., 2000; Jockusch and Voigt, 2003; Kuang et al., 2007; Siegel et al., 2009). For example, time-lapse imaging in a 3D myofiber culture system has shown that activated satellite cells are highly dynamic and migrate along the muscle fiber by extending unipolar or bipolar cellular protrusions (Siegel et al., 2009). However, muscle stem cells that are separated from their physiological environment are invariably activated, and *in vitro* approaches therefore do not provide the whole picture of their endogenous behavior. With the advance of intravital imaging, recent work provides the first glimpse of mouse satellite cell behavior *in vivo* (Webster et al., 2016). Quiescent satellite cells are largely immobile, while activated satellite cells proliferate and migrate along the ECM remnants of injured myofibers during regeneration. This work highlights the importance of *in vivo* approaches to study muscle stem cells.

The remarkable regenerative ability and the ease of *in vivo* imaging have made zebrafish a powerful system to study muscle stem cell behavior (Ratnayake and Currie, 2017). The zebrafish dermomyotome, also known as the external cell layer (ECL), is marked by the expression of *pax3* and *pax7*, similar to higher vertebrates (Devoto et al., 2006; Feng et al., 2006; Hammond et al., 2007). During somitogenesis, *pax3/pax7*$^{+}$ dermomyotome is generated from the anterior somitic compartment through whole-somite rotation and is thought to generate new muscle fibers during myotome growth (Hollway et al., 2007; Stellabotte et al., 2007). At 4-5 days post-fertilization (dpf), some *pax7*$^{+}$ muscle progenitor cells can be observed deep in the myotome between muscle fibers (Seger et al., 2011). Therefore, *pax7* labels at least two populations of muscle progenitor cells in zebrafish embryos: first embryonic muscle progenitor cells in the dermomyotome on the surface of the somite, and later fiber-associated deep myotomal cells, some of which have been shown to be functionally equivalent to mammalian satellite cells (Gurevich et al., 2016). Although *pax7*$^{+}$ muscle progenitor cells have been shown to contribute to muscle injury repair (Gurevich et al., 2016; Knappe et al., 2015; Pipalia et al., 2016; Seger et al.,

2011), the behavior and contribution of early muscle progenitor cells from the dermomyotome has not been specifically explored due to the lack of specific reporters.

In this study, we developed new transgenic tools and methods to analyze the dynamics of dermomyotome cells at single cell resolution. We identified a number of ECM genes as new markers of dermomyotome cells. Genetic lineage tracing using *col1a2*-based transgenic lines demonstrated that dermomyotome cells contribute not only to embryonic muscle growth but also to injury repair. Using *in vivo* imaging and single cell clonal analysis, we described the dynamics of “quiescent” and “activated” dermomyotome cells. Together, our study provides a dynamic view of embryonic muscle progenitor cells during muscle homeostasis.

RESULTS

Extracellular matrix genes are enriched in the dermomyotome

The dermomyotome in zebrafish is traditionally labeled by expression of the muscle progenitor cell marker *pax7* (Devoto et al., 2006; Feng et al., 2006; Hammond et al., 2007). Using double fluorescent in situ hybridization, we identified several extracellular matrix (ECM) genes, including *col1a2* (*collagen 1a2*), *col5a1* (*collagen 5a1*) and *cilp* (*cartilage intermediate layer protein*), that showed co-expression with *pax7* in the dermomyotome on the outer surface of the somite (Fig. 1A). To visualize the dynamics of dermomyotome cells *in vivo*, we generated a *col1a2:Gal4* transgenic line by BAC (bacteria artificial chromosome) recombineering (Fig. 1B). The *col1a2:Gal4* line can be crossed with different UAS lines to label, ablate, or lineage trace dermomyotome cells. Co-labeling using *col1a2* and *kaede* probes in *col1a2:Gal4; UAS:Kaede* (*col1a2*^{Kaede} in short) embryos revealed that the *col1a2:Gal4* reporter largely recapitulated the endogenous *col1a2* expression pattern (Fig. S1). Similarly, *col1a2:Gal4; UAS:NTR-mCherry* (*col1a2*$^{NTR\text{-}mCherry}$ in short) labeled the outer surface of the somite external to *α-actin:GFP*-expressing muscle cells, corresponding to the anatomical location of the dermomyotome (Fig. 1C and Movie 1). The labeling of a few muscle fibers by *col1a2*$^{NTR\text{-}mCherry}$ suggests that *col1a2*$^{+}$ cells contribute to muscle fiber formation. To confirm that the *col1a2:Gal4* line labels the dermomyotome, we performed immunostaining using the anti-Pax7 antibody in *col1a2*$^{NTR\text{-}mCherry}$ embryos at 2 dpf. Pax7 antibody labels both dermomyotome cells (weaker staining) and xanthophores, neural crest-derived pigment cells (stronger staining). Indeed, all *mCherry*$^{+}$ cells on the lateral surface of the somite were weakly *Pax7*$^{+}$ (Fig. 1D), indicating that *col1a2*$^{NTR\text{-}mCherry}$ specifically labels the dermomyotome but not xanthophores. To determine whether the dermomyotome is present in adult zebrafish, we imaged vibratome sections of *col1a2*$^{NTR\text{-}mCherry}$ fish at 22 mm SL (standard length). We identified three layers of *col1a2*$^{+}$ cells external to the muscles, corresponding to scales (the most outer layer), skin (the middle layer), and the presumptive dermomyotome (the most inner layer external to muscles) (Fig. 1E). The presence of a few *mCherry*$^{+}$ muscle fibers adjacent to the presumptive dermomyotome suggests that dermomyotome cells contribute to muscle growth in adult zebrafish.

147 **Characterization of the dermomyotome**

148 Using the *col1a2:Gal4* line, we determined the number, distribution, morphology, and
149 dynamics of dermomyotome cells. To quantify the number of dermomyotome cells, we first
150 performed Pax7 antibody staining in *col1a2*$^{NTR\text{-}mCherry}$ embryos at 2 dpf. On average, there
151 were 25 *Pax7*$^{+}$ dermomyotome cells per somite, of which about 87% were also *col1a2*$^{+}$ (Fig.
152 2A), suggesting that the *col1a2*$^{NTR\text{-}mCherry}$ line labels most dermomyotome cells. The
153 incomplete labeling likely reflects the variegated nature of the Gal4-UAS system (Akitake et
154 al., 2011). Second, *col1a2*$^{+}$ dermomyotome cells appeared to distribute evenly to cover the
155 entire surface of the somite (Fig. 1D). About 42% of cells were located along the vertical
156 myoseptum, 43% in between somite boundaries, and 15% along the horizontal myoseptum
157 (Fig. 2B,C). Third, by taking advantage of some highly mosaic *col1a2*^{Kaede} embryos, we were
158 able to visualize the morphology of individual dermomyotome cells at 3 dpf (Fig. 2D). They
159 were relatively flat cells sandwiched between the epithelium and muscle fibers. Individual
160 *col1a2*$^{+}$ dermomyotome cells appeared to either "float" in between the two somite boundaries
161 or "anchor" their cell bodies along the myoseptum. They always exhibited a remarkable
162 ramified morphology with multipolar lamellipodia-like cellular projections (Fig. 2D). Thin
163 cellular projections (up to 10 μm) extending out of these lamellipodia can often be observed
164 in *col1a2*$^{+}$ cells, suggesting potential long range cell-cell communications or the ability to
165 detect distant injuries. By combining two UAS reporters, we visualized the dynamics of
166 dermomyotome cells in *col1a2:Gal4; UAS:NTR-mCherry; UAS:Kaede* embryos (Fig. 2E). The
167 mosaic nature of these transgenes allowed us to label a large number of dermomyotome
168 cells in different colors. Dermomyotome cells appeared to evenly cover the surface of the
169 somite with each cell occupying a non-overlapping territory. Time-lapse imaging showed that
170 after cell division, daughter cells regained the ramified morphology and maintained the similar
171 territory previously occupied by the mother cell (Fig. 2E and Movie 2). Together, our results
172 demonstrate that the new *col1a2:Gal4* driver can be utilized to visualize the dynamics of
173 dermomyotome cells at single cell resolution in zebrafish.
174
175 **Dermomyotome cells generate new muscle fibers during embryonic muscle growth**
176 To determine whether the dermomyotome contributes to muscle growth, we performed
177 two different lineage tracing experiments to follow *col1a2*$^{+}$ dermomyotome cells. In the first

approach, we took advantage of the photoconvertible fluorescent protein, Kaede (Ando et al., 2002). The normally green-fluorescent Kaede protein (*Kaede*^{green}) can be photoconverted to a red-fluorescent Kaede protein (*Kaede*^{red}) by UV light. The perdurance of the *Kaede*^{red} protein allows us to trace Kaede-expressing cells for multiple days during development. Briefly, we photoconverted a region of 5-6 somites in *col1a2*^{Kaede} embryos at 3 dpf, labeling *col1a2*$^{+}$ dermomyotome cells with *Kaede*^{red} (Fig. 3A). We then imaged the converted region of the same fish 24 and 48 hours later. New muscle fibers can be easily identified based on their elongated morphology spanning the entire somite between two adjacent vertical myosepta. The emergence of new *Kaede*^{red} muscle fibers suggests that *col1a2*$^{+}$ dermomyotome cells contribute to new muscle fibers during normal larval development (Fig. 3B).

As a complementary approach, we performed Cre-mediated lineage tracing to determine the fate of *col1a2*$^{+}$ dermomyotome cells. We generated the *col1a2:Gal4; UAS:Cre-ERT2* (*col1a2*$^{Cre\text{-}ERT2}$ in short) transgenic line to express tamoxifen-inducible Cre recombinase in dermomyotome cells, and utilized the *ubi:loxP-EGFP-loxP-mCherry* (*ubi:Switch*) line (Mosimann et al., 2011) as the lineage reporter. Induction of Cre activity by 4-hydroxytamoxifen (4-OHT) results in the excision of the EGFP cassette and subsequent expression of the mCherry protein in the cell and its progeny (Fig. 3C). *col1a2*$^{Cre\text{-}ERT2}$*; ubi:Switch* embryos were treated with 4-OHT for 2 hours at 3 dpf and imaged every 24 hours thereafter. At 24 hours after 4-OHT pulse, *col1a2*$^{+}$ dermomyotome cells were mosaicly labeled by the mCherry expression, but no muscle fibers were labeled (Fig. 3D). Tracing of *mCherry*$^{+}$ dermomyotome cells for 4 consecutive days revealed that new *mCherry*$^{+}$ muscle fibers started to emerge at 48 hours post 4-OHT pulse, and increased in number at later time points. Thus, consistent with Kaede-based lineage tracing experiments, this result confirms that dermomyotome cells contribute to the generation of new muscle fibers during muscle homeostasis.

ECM dynamics during muscle regeneration

We have shown above that *col1a2*$^{+}$ dermomyotome cells express muscle progenitor marker *pax7* and contribute to normal muscle growth. To determine whether they also contribute to muscle regeneration, we performed needle injury experiments on muscles of *col1a2*$^{NTR\text{-}mCherry}$*; α-actin:GFP* embryos (Fig. 4A). Fish were injured within a 1-2 somite area

at 3 dpf and imaged every 24 hours for 3 days. At 24 hpi (hours post injury), the injury area, as indicated by the absence of *α-actin:GFP* expression, became substantially smaller than that at 1 hpi. This was accompanied by the emergence of elongated *mCherry*$^{+}$ cells in the *GFP*$^{-}$ area, suggesting that *col1a2*$^{+}$ dermomyotome cells were recruited to the injury site. By 48 hpi, the injury area was completely replaced by newly regenerated muscles, as indicated by higher level of *α-actin:GFP* expression compared to uninjured regions. At 72 hpi, some newly formed muscles were also labeled by *mCherry* expression, suggesting that they were derived from *col1a2*$^{+}$ dermomyotome cells. Thus, needle injury experiments demonstrate that small muscle injuries can be quickly repaired within 48 hours in zebrafish and *col1a2*$^{+}$ dermomyotome cells are likely the source of new muscle fibers.

We further investigated the expression kinetics of different markers during the entire process of muscle injury repair. Fish were injured by needle stabbing at 3 dpf, and fixed at different time points (7, 24, 48, 76 hpi) for in situ analysis (Fig. 4B). The expression of the muscle stem cell marker *pax7* reached the highest level at the injury site at 24 hpi. The elevated *pax7* expression remained at 48 hpi before returning back to the basal level by 76 hpi. By contrast, myogenic markers (*myoD* and *myogenin*) displayed a kinetics slightly lagging behind *pax7*. Their expression initiated at 24 hpi, reached the peak level at 48 hpi, and returned to the basal level by 76 hpi. This result is consistent with the timing of muscle regeneration from the activation of muscle progenitor cells to the differentiation of new muscle fibers (Fig. 4A). Lastly, analysis of several ECM genes (*col1a2*, *col5a1*, *col1a1a*, *cilp*, *postnb* and *sparc*) revealed similar expression kinetics as *pax7* (Figs 4B and S2). The expression of ECM genes was strongly induced at the injury site at 24 hpi and then gradually declined in the following 48 hours. Together, our results suggest that dermomyotome cells not only are recruited to the injury site to generate new muscle fibers, but also upregulate ECM gene expression perhaps to facilitate the repair.

Single cell dynamics of dermomyotome cells

We have shown that dermomyotome cells generate new muscle fibers during both normal muscle growth and muscle injury repair. To define the dynamic behavior of individual dermomyotome cells *in vivo*, we performed single cell clonal analysis by taking advantage of the photoconvertible Kaede and the mosaic nature of the *col1a2*^{Kaede} transgenic line.

Photoconversion of one isolated *Kaede*^{green} dermomyotome cell allowed us to visualize its cellular behavior and trace all of its *Kaede*^{red} descendants. Briefly, we screened *col1a2*^{Kaede} fish at 3 dpf and identified embryos with mosaic labeling of the dermomyotome. Single isolated *Kaede*^{green} cells were photoconverted with one cell per somite (3-4 cells per embryo) to ensure accurate cell tracing across multiple time points. We then used the two-photon laser to introduce targeted muscle injury near one *Kaede*^{red} cell. *Kaede*^{red} dermomyotome cells in laser ablated somites were referred to as cells under injured condition, whereas photoconverted cells in uninjured somites were defined as control cells under wild-type condition. Individual embryos were imaged at 1, 24, 48, and 72 hpi to capture the dynamics of individual converted cells and their descendants (Fig. 5A).

Based on cell behaviors of each clone, we categorized the response of dermomyotome cells into four different categories (Fig. 5B). In type I response, cells did not proliferate and maintained the ramified morphology throughout 72 hours. In type II response, cells underwent one or more cell divisions, but all daughters maintained the ramified morphology, suggesting a quiescent state. By contrast, in type III response, cells generated small elongated cells, which were usually bi-polar with processes extending along muscle fibers. This is markedly distinct from the multipolar ramified morphology of quiescent dermomyotome cells, suggesting an activated state. Lastly, in type IV response, cells first gave rise to small elongated cells similar to those in the type III response, some of which later generated one or more *Kaede*^{red} muscle fibers by 72 hpi. As Kaede protein appeared to concentrate in the nuclei of muscle cells (Fig. S3A), new muscle fibers generated from *Kaede*^{red} cells can be easily identified based on the stronger *Kaede*^{red} signal in the oval-shaped nucleus with a weaker and diffusive signal in the cytoplasm spanning the width of a somite. Antibody staining confirmed that the *Kaede*^{red} nucleus of a newly generated muscle no longer expressed Pax7, a feature typical of differentiated muscles, whereas small elongated cells remained *Pax7*$^{+}$ (Fig. S3B). Together, under wild-type conditions, dermomyotome cells generated predominantly type I (59%, 38/65 cells) or type II (40%, 26/65 cells) responses, but rarely type III response (2%, 1/65 cells) and never type IV response (Fig. 5C). By contrast, cells under injured conditions exhibited all four types of responses, with a combined 35% (24/68 cells) in the type III and IV categories. Similarly, 24% (16/68 cells) of dermomyotome cells in injured condition generated clones of at least 3 cells

compared to only 2% (1/65 cells) in wild-type conditions (Fig. S3C), suggesting an increase in cell proliferation during muscle injury repair. These results suggest that type III/IV behaviors represent the muscle regenerative response of "activated" dermomyotome cells. Since the formation of new muscle fibers was always preceded by small elongated cells (Fig. 5B), the type III response likely represents a transitional phase before the formation of new muscle fibers (type IV response).

Since not all dermomyotome cells would respond to the injury in the same somite (Fig. 5B,C), we asked whether the initial position of the cell influences its behavior. We found that the distance from the injury to the center of the labeled cells does not correlate with the type of response (Fig. 5D). For example, some cells at 24 μm away failed to respond to the injury, while some other cells over 80 μm away became activated. This result suggests that dermomyotome cells can detect and respond to an injury at a long distance away from the cell body. Interestingly, dermomyotome cells located along the myoseptum are more likely to generate a type III or IV response (52%, 12/23 cells) than centrally located cells (29%, 13/45 cells) (Fig. 5E), suggesting that the local niche might influence the behavior of muscle progenitor cells.

New muscle fibers are predominantly generated by fusion

Our single cell lineage tracing experiments indicate that "activated" dermomyotome cells go through a series of stereotypic phases to generate new muscle fibers (Fig. 5). To further confirm this, we carried out confocal time-lapse imaging to visualize the entire process of muscle regeneration. First, we imaged the "early phase" of muscle repair between 0 to 24 hpi (Fig. 6A). Moderately mosaic *col1a2*^{Kaede} embryos were injured by needle stabbing at 59 hpf. Isolated *Kaede*^{green} cells were photoconverted to facilitate cell tracking (Fig. 6B and Movie 3). Within the first 24 hours, the "activated" dermomyotome cell started to project polarized cellular processes along muscle fibers. This bi-polar and elongated morphology was maintained even after the cell division. Consistent with our previous observations, new muscle fibers were rarely generated during this time interval. Thus, the "early phase" of muscle regeneration is characterized by the morphological changes and proliferations of "activated" dermomyotome cells. Next, we performed time-lapse imaging of the "late phase" of muscle injury repair. Mosaic *col1a2*^{Kaede} embryos were injured by needle stabbing at 3 dpf

and imaged from 29 to 48 hpi (Fig. 6C). From a total of 9 movies collected, we observed the generation of 13 new muscle fibers. Remarkably, all 13 fibers were formed in a similar fashion: a small elongated *Kaede*$^{+}$ cell at one time point disappeared by the next time point (8-minute intervals), with simultaneous emergence of *Kaede*$^{+}$ muscle fiber characterized by *Kaede*^{strong} nucleus and *Kaede*^{weak} cytoplasm (Fig. 6D). The rapidity of this event suggests that new muscle fibers are formed through cell fusions between a *Kaede*$^{+}$ dermomyotome derived cell and an existing non-labeled muscle fiber.

Since we never observed any *de novo* fiber formation in our time-lapse movies, we asked whether muscles are formed only through cell fusions. To answer this question, we performed genetic lineage tracing in the *col1a2*$^{Cre\text{-}ERT2}$*; ubi:Switch* fish (Fig. 7A). Embryos at 3 dpf were treated with 4-OHT for 3.5 hours to mosaicly label dermomyotome cells. Fish were then injured by needle stabbing and imaged at 75 hpi to quantify newly formed *mCherry*$^{+}$ muscle fibers. If a new muscle fiber is generated *de novo*, it would be *mCherry*$^{+}$ but *EGFP*$^{-}$ due to the excision of the EGFP cassette by Cre-mediated switching. Conversely, if an *mCherry*$^{+}$ dermomyotome cell fuses with an already existing muscle fiber (*EGFP*$^{+}$), the resulting new muscle fiber will express both mCherry and EGFP (Fig. 7B). In uninjured control embryos, 97% of new muscle fibers (37/38) were formed via cell fusion, whereas only 3% of fibers (1/38) were generated *de novo* (Fig. 7C,D). Interestingly, in injured embryos, *de novo* fiber formation increased slightly to 14% (14/98) at the muscle injury site. Together, this result is consistent with our time-lapse imaging that new muscle fibers are generated predominantly through cell fusion of dermomyotome descendants with existing muscle fibers.

Dermomyotome cells are required for effective muscle regeneration

To test whether dermomyotome cells are essential for embryonic muscle injury repair, we ablated *col1a2*$^{+}$ dermomyotome cells using the nitroreductase (NTR) based system. The NTR enzyme converts the harmless prodrug metronidazole (MTZ) into a cytotoxic compound that induces rapid cell death of NTR-expressing cells (Curado et al., 2008; Pisharath et al., 2007). *col1a2*$^{NTR\text{-}mCherry}$ or sibling control embryos were treated with MTZ from 2 to 3 dpf, injured at 3 dpf, and fixed at 24 hpi for in situ analysis (Fig. 7E). In control embryos, *myoD* expression was significantly upregulated at the site of injury (Fig. 7F), suggesting a robust regenerative response. By contrast, most MTZ-treated *col1a2*$^{NTR\text{-}mCherry}$ embryos showed no

specific induction of *myoD* at the injury site. This result suggests that *col1a2*$^{+}$ dermomyotome cells are required for an efficient muscle injury repair in early zebrafish embryos.

DISCUSSION

Using zebrafish as a model, our study provides a dynamic view of embryonic muscle progenitor cells in the dermomyotome. First, dermomyotome cells display a unique ramified morphology expressing many ECM genes. Second, lineage tracing experiments show that dermomyotome cells contribute to normal muscle growth as well as muscle injury repair. Third, dermomyotome cells undergo a series of stereotypical steps to generate new muscle fibers, predominantly by cell fusion with existing fibers.

Dermomyotome cells are embryonic muscle progenitor cells

Dermomyotome is an evolutionarily conserved structure on the external surface of the myotome present in most vertebrates (Devoto et al., 2006). In zebrafish, the dermomyotome displays remarkable similarities to that of higher vertebrates. Our work and that of others (Devoto et al., 2006; Feng et al., 2006; Hammond et al., 2007) show that the dermomyotome occupies a similar domain on the surface of each somite and expresses the muscle progenitor cell marker *pax7*. Previous work in mouse and chick has shown that satellite cells originate from the embryonic dermomyotome (Gros et al., 2005; Kassar-Duchossoy et al., 2005; Relaix et al., 2005; Schienda et al., 2006). Consistent with this, using lineage tracing and time-lapse imaging, we showed that *col1a2*$^{+}$ dermomyotome cells contribute to not only new muscle fibers but also small *pax7*$^{+}$ fiber-associated cells, likely corresponding to larval muscle progenitor cells (Gurevich et al., 2016; Nguyen et al., 2017; Pipalia et al., 2016; Roy et al., 2017; Seger et al., 2011).

We also observed some differences between zebrafish and higher vertebrates. First, in mouse and chick, the dermomyotome has been shown to give rise to both muscles and the dermis (Christ and Scaal, 2008; Stellabotte and Devoto, 2007). Interestingly, we did not observe any contribution of *col1a2*$^{+}$ dermomyotome cells to the dermis in cell tracing experiments. One possible explanation is that *col1a2*$^{+}$ dermomyotome cells are already committed to the myogenic lineage by the time our *col1a2* reporters are expressed at high level in the dermomyotome at 2 dpf. Indeed, dye labeling of early dermomyotome precursors in the anterior somitic compartment prior to the somite rotation marks both muscles and some dermal-like cells (Hollway et al., 2007). Second, we found that the zebrafish dermomyotome

366 persists in adults, similar to previous observations of *pax7* and *pax3* expression on the lateral
367 surface of adult myotomes (Hollway et al., 2007; Nguyen et al., 2017). This persistence is in
368 contrast with the amniotic dermomyotome, which is shown to be a transient embryonic
369 structure (Christ and Scaal, 2008; Stellabotte and Devoto, 2007). The presence of the
370 dermomyotome in adult zebrafish is likely required for the continuous growth of the fish.
371
372 **Unique morphology of dermomyotome cells**
373 Using *col1a2* transgenic lines, we identified several new features of dermomyotome cells.
374 First, dermomyotome cells display a ramified morphology. In a quiescent state, these cells
375 are not polarized, with lamellipodia-like structures all around the cell. This morphology is in
376 contrast with mouse satellite cells, which usually display a bipolar morphology with short
377 processes extending along the myofiber (Webster et al., 2016). Second, although
378 dermomyotome cell bodies are mostly stationary in uninjured conditions, their cellular
379 processes are quite dynamic, constantly extending and retracting. Each cell and its
380 processes occupy a largely non-overlapping area, reminiscent of the tiling of neuronal
381 dendrites (Grueber and Sagasti, 2010). During cell division, the mother cell retracts all its
382 processes, but immediately after the division, the two daughter cells would extend new
383 processes to reclaim the similar surface area. These dynamic behaviors might ensure the
384 complete coverage of the somitic surface and detect potential muscle injuries. Lastly, we
385 often observed long filopodia-like structures extending from dermomyotome cells. Intriguingly,
386 our single cell lineage analysis revealed that the distance between the dermomyotome cell
387 body and the injury site is not a reliable predictor of whether the cell would generate a
388 regenerative response. It thus raises the possibility that the long cellular projections might
389 allow the dermomyotome cell to detect muscle injury at a significant distance away from the
390 cell body. Consistent with our findings, dermomyotome cells in chick display similar filopodia-
391 like protrusions, facilitating the interaction with the overlying ectoderm during somite
392 development (Sagar et al., 2015).
393
394 **ECM genes as novel markers of dermomyotome cells**
395 The dermomyotome is traditionally defined by muscle progenitor cell markers *pax7* and
396 *pax3*. We demonstrated that the zebrafish dermomyotome expresses a number of ECM

genes, including *col1a2*, *col5a1*, and *cilp*. Consistent with our finding, an ultrastructural expression analysis in zebrafish identifies some *col1a2*$^{+}$ mesenchymal cells on the surface of muscles, likely corresponding to dermomyotome cells (Le Guellec et al., 2004). Similarly, *col1a1* and *cilp* have been shown to express in a dermomyotome-like domain in trout embryos (Ralliere et al., 2015; Rescan et al., 2005). Moreover, we found that the expression of these ECM genes is dynamically induced during muscle injury repair. Our observations in embryonic muscle progenitor cells in zebrafish show strong similarities to mouse muscle progenitor cells. For example, fetal muscle stem cells in mice show high-level expression of several ECM molecules, such as tenascin-C (*TnC*), fibronectin (*Fn1*), and collagen VI (*Col6*) (Tierney et al., 2016). Similarly, newly identified *Twist2*$^{+}$ mouse muscle progenitor cells show enrichment in many ECM genes, including *Col1a1*, *Col1a2*, and *Cilp* (Liu et al., 2017). Interestingly, although quiescent adult satellite cells do not express high level of ECM genes (Liu et al., 2017), activated satellite cells show upregulation of many collagen genes, such as *Col1a1* and *Col1a2* (Pallafacchina et al., 2010). Thus, dynamic regulation of ECM gene expression might be a common feature of muscle progenitor cells.

Does the ECM play an active role in regulating the function of dermomyotome cells? We envision two non-mutually exclusive scenarios. First, the ECM might be an integral part of the niche in maintaining the self-renewing property of muscle progenitors. Recent work has implicated many ECM components, including fibronectin, tenascin-C, laminins, and collagens, as critical niche factors that modulate satellite cell function (Bentzinger et al., 2013b; Fry et al., 2017; Rayagiri et al., 2018; Tierney et al., 2016; Urciuolo et al., 2013). In particular, it has been shown that Collagen V produced by adult muscle satellite cells is an essential component of the quiescent niche, as deletion of the *Col5a1* gene results in depletion of the stem cell pool (Baghdadi et al., 2018). Second, the induction of ECM gene expression upon muscle injury might provide the appropriate scaffold for the recruitment and/or migration of activated muscle progenitor cells. Consistent with this idea, intravital imaging of muscle regeneration in mice reveals that ECM remnants from injured muscle fibers provides cues to regulate muscle progenitor cell behavior (Webster et al., 2016). It remains to be investigated whether loss of any ECM component would compromise the regenerative capacity of dermomyotome cells in zebrafish.

428 **Single cell dynamics of dermomyotome cells during injury repair**

429 The existing *pax7* reporters in zebrafish label not only the dermomyotome and the
430 overlying xanthophores, but also fiber-associated deep myotomal cells (Pipalia et al., 2016;
431 Seger et al., 2011), which makes imaging individual dermomyotome cells challenging. To
432 circumvent this issue, we developed a new *col1a2:Gal4* transgenic line to label and image
433 dermomyotome cells. By taking advantage of the variegated nature of the *col1a2:Gal4;*
434 *UAS:Kaede* line and the photoconvertible Kaede, we performed single cell clonal analysis of
435 dermomyotome cells. A "quiescent" dermomyotome cell (type I/II responses) maintains its
436 ramified morphology even after occasional cell divisions. By contrast, an "activated"
437 dermomyotome cell (type III/IV responses) undergoes several stereotypic steps to generate
438 new muscle fibers (Fig. 7G). First, it changes from its resting ramified morphology to an
439 elongated and polarized morphology, usually within the first 3-5 hours after injury. The cell
440 extends long cellular projections along the longitudinal axis of neighboring muscle fibers.
441 Next, the "activated" cell undergoes several rounds of cell divisions generating a clone of
442 small polarized daughter cells by 12-24 hpi. Finally, by 72 hpi, new muscle fibers emerge at
443 the injury site, likely formed through fusion with uninjured muscle fibers (discussed below).
444 The dynamic behaviors of an "activated" dermomyotome cell, such as the initial polarization
445 phase, are reminiscent of *myf5*$^{+}$ fiber-associated muscle progenitor cells during muscle
446 regeneration (Gurevich et al., 2016). Interestingly, unlike *myf5*$^{+}$ muscle progenitor cells,
447 dermomyotome cells do not cross the myotendinous junction to repair muscle injury in
448 neighboring somites. Quantification of our single cell clonal analysis further reveals that
449 although the distance to the injury does not predict the response of the dermomyotome cell
450 (discussed above), dermomyotome cells located along myosepta are more likely to respond
451 to the injury than centrally located ones. This result suggests that ECM-enriched
452 myotendinous junction might provide the scaffold to facilitate the migration of activated
453 dermomyotome cells.
454
455 **Dermomyotome cells generate new fibers by fusion**
456 Two independent lines of evidence indicate that dermomyotome cells generate new
457 muscle fibers primarily through cell fusion. First, time-lapse imaging of the regeneration
458 process in *col1a2*^{Kaede} embryos showed that the emergence of *Kaede*$^{+}$ muscle fiber always

appeared to be completed between two time points (8-minute interval), accompanied by the simultaneous disappearance of the dermomyotome cell. The absence of intermediate steps, such as searching for attachment sites along the myotendinous junction, suggests that new fibers are formed by cell fusion rather than *de novo* fiber formation. Second, our Cre-mediated lineage tracing experiments showed that most new muscle fibers express both EGFP and mCherry, indicating cell fusion events between a switched dermomyotome cell (*mCherry*$^{+}$, *ubi:loxP-mCherry*) and an un-switched muscle fiber (*EGFP*$^{+}$, *ubi:loxP-EGFP-loxP-mCherry*). Intriguingly, during muscle injury repair, significantly more *de novo* fiber formation (14%) was observed compared to uninjured conditions (3%). This discrepancy might be explained by differential activation of sub-populations of dermomyotome cells. Recent work shows that two paralogues of *pax7*, *pax7a* and *pax7b*, mark similar but not identical muscle progenitor cell populations. *pax7b*$^{+}$ cells contribute to muscle growth and repair by cell fusions, whereas *pax7a*$^{+}$*pax7b*$^{-}$ cells predominantly generate nascent fibers (Pipalia et al., 2016). Our results suggest that normal muscle growth is primarily contributed by *pax7b*$^{+}$ dermomyotome cells, while muscle injury activates both *pax7b*$^{+}$ and *pax7a*$^{+}$*pax7b*$^{-}$ cells. Consistent with this idea, *pax7a*$^{+}$ cells have been shown to contribute to only large muscle injuries but not small injuries (Knappe et al., 2015).

In summary, our work provides a dynamic view of dermomyotome cells during muscle growth and repair. It also raises additional questions for future investigations. For example, what is the injury signal that activates dermomyotome cells? Tissue injury is often associated with elevated level of reactive oxygen species (ROS) and the recruitment of patrolling immune cells such as macrophages and neutrophils (Love et al., 2013; Niethammer et al., 2009). It is therefore plausible that ROS and/or cytokines secreted by immune cells might be the trigger to activate dermomyotome cells. Indeed, mice and human data have implicated macrophages and other immune cells as the critical regulators of satellite cell functions (Bentzinger et al., 2013a; Saclier et al., 2013).

MATERIALS AND METHODS

Zebrafish strains

Zebrafish strains were maintained and raised according to the standard protocols (Westerfield, 2000). All procedures were approved by the University of Calgary Animal Care Committee. Embryos were grown at 28.5 °C and staged as previously described (Kimmel et al., 1995). Fish older than 24 hpf were treated with 1-phenyl 2-thiourea (PTU) to prevent pigmentation. TL and TL/AB wild-type strains were used in this study along with the following transgenic lines: *α-actin:GFP* (Higashijima et al., 1997), *col1a2:Gal4*, *UAS:Kaede* (Scott et al., 2007), *UAS:NTR-mCherry* (Davison et al., 2007), *UAS:Cre-ERT2*, *Ubi:loxP-EGFP-loxP-mCherry* (*Ubi:Switch*) (Mosimann et al., 2011). The mosaic *col1a2:Gal4; UAS:Kaede* line was maintained by selectively growing embryos with more mosaic Kaede expression.

Generation of transgenic lines

UAS:Cre-ERT2 was generated by standard Tol2-mediated transgenesis. To generate *col1a2:Gal4* transgenic line, BAC clone zC122K13 from the CHORI-211 library that contains *col1a2* genomic region with 78 kb upstream and 58 kb downstream regulatory sequences was selected for bacteria mediated homologous recombination following the standard protocol (Bussmann and Schulte-Merker, 2011). Briefly, the pRedET plasmid was first transformed into BAC-containing bacteria. Second, an iTol2_amp cassette containing two Tol2 arms in opposite directions flanking an ampicillin resistance gene was recombined into the vector backbone of zC122K13. Lastly, a cassette containing the Gal4-VP16 with a kanamycin resistant gene was recombined into zC122K13-iTol2_amp to replace the first coding exon of the *col1a2* gene. After each round of recombination, successful recombinants were confirmed by PCR analysis. The final *col1a2:Gal4* BAC was then co-injected with *tol2* transposase mRNA into *UAS:Kaede* embryos at one-cell stage. Positive transgenic lines were identified by screening Kaede expression in F1 embryos from injected founders.

Muscle injury

Two methods were employed to generate muscle injury at specific locations in larval zebrafish. In needle injury, we used a sharp injection needle to stab muscles near the end of

yolk extension (somites 17-19) so the injury site can be recognized easily during the lineage tracing. Alternatively, to introduce muscle injury at a more precise location, laser ablation was performed with the 750 nm laser and the 25x objective on the Leica TCS SP8 multi-photon microscope. A region of interest (ROI) at a desired location was selected, zoomed in to the maximum (48x), and scanned with 100% 750 nm laser once. The laser-induced injury can be readily visualized in the bright field after the scanning.

Kaede photoconversion

col1a2^{Kaede} embryos at appropriate stages were anesthetized with tricaine and mounted in 0.8% low melting point agarose in a glass bottom dish (MatTek). Photoconversion experiments were performed using the 405 nm laser and the 20x objective on the Olympus FV1200 confocal microscope. For photoconversions of large areas (~ 5 to 6 somite region), 50% laser power was used to scan the desired ROI for 2 frames at a dwell time of 200 μs per pixel. For single cell photoconversions, 2% laser power was used to scan a small ROI (10 x 10 pixels) with the Tornado mode at a dwell time of 2 μs per pixel for a total of 1-2 seconds. After photoconversion, embryos were released from the agarose, transferred to fish water to recover in the dark, and analyzed at desired stages.

Cre-mediated lineage tracing

To obtain mosaic labeling, *col1a2:Gal4; UAS:Cre-ERT2; ubi:Switch* embryos were pulsed with 10 μM 4-hydroxytamoxifen (4-OHT) for 2-3 hours at desired stages. After treatment, 4-OHT was washed off with fish water for three times, and embryos were recovered in fish water for analysis at appropriate stages.

Single cell lineage tracing

Mosaic *col1a2*^{Kaede} embryos at appropriate stages were selected for single cell tracing experiments. Individual isolated cells were photoconverted to *Kaede*^{red}. To ensure reliable cell tracing over time, a maximum of one cell per somite and four cells per embryo were photoconverted and traced. Immediately after photoconversion, muscle injury was introduced by laser ablation near one *Kaede*^{red} cell. Images were taken before and after the photoconversion and then every 24 hours till 72 hpi to trace individual *Kaede*^{red} cells. For

548 quantification in Fig. 7D, distance was measured from the center of the photoconverted cell to
549 the center of the muscle injury.
550
551 **In situ hybridization and immunohistochemistry**
552 Whole-mount in situ hybridization and antibody staining were performed according to the
553 standard protocols (Thisse et al., 2004). The following antisense probes were used in this
554 study: *cilp*, *col1a1a*, *col1a2*, *col5a1*, *kaede*, *myoD*, *myogenin*, *pax7* (Seo et al., 1998), *postnb*
555 and *sparc*. For antibody staining, the following primary antibodies were used: rabbit
556 polyclonal antibody to Kaede (1:1000, MBL) and mouse monoclonal antibody to Pax7 (1:10,
557 Developmental Studies Hybridoma Bank (DSHB)). For fluorescent detection of antibody
558 labeling, appropriate Alexa Fluor-conjugated secondary antibodies (1:500, Molecular Probes)
559 were used.
560
561 **Cell ablation experiments**
562 To ablate *col1a2*$^{+}$ cells, *col1a2*$^{NTR\text{-}mCherry}$ transgenic fish were outcrossed with wild-type
563 fish to obtain *mCherry*$^{+}$ embryos (experimental group) and *mCherry*$^{-}$ embryos (control group).
564 Embryos at 48 hpf were treated with metronidazole (MTZ) at a final concentration of 5 mM in
565 fish water for 24 hours. Embryos were then washed with E3 fish water 2-3 times and grown to
566 desired stages for analysis.
567
568 **Time-lapse imaging and processing**
569 Embryos were anesthetized with tricaine and embedded in 0.8% low melting point
570 agarose on a glass bottom dish (MatTek). Fish were imaged with Olympus FV1200 confocal
571 microscope using the 20x objective. For time-lapse imaging of muscle injury repair, embryos
572 were first injured at 3 dpf either by needle stabbing or laser ablation. Injured embryos were
573 then imaged laterally starting at either 0 or 29 hpi at 8-min intervals for 19-20 hours. All the
574 confocal images were analyzed and quantified using the Fiji software (Schindelin et al.,
575 2012). Brightness and contrast were adjusted for better visualization. To generate color-
576 coded depth projections, confocal z-stacks were processed with Fiji using the 'temporal color
577 code' function.
578

579 **Quantification of dermomyotome cells**

580 *col1a2*$^{NTR\text{-}mCherry}$ fish were stained with anti-Pax7 antibody at 2 dpf. Cells in each somite
581 were counted based on *col1a2* expression and Pax7 staining: all Pax7^{+} cells, Pax7^{+}Col1a2^{+}
582 cells and Pax7^{+}Col1a2^{-} cells. Note that xanthophores, which have strong Pax7 staining, were
583 not counted. Overall, average number of cells in five somites per embryo was used for the
584 quantification. Pax7^{+}Col1a2^{+} cells were further categorized according to their position in a
585 somite: near the vertical myosepta (VM), near the horizontal myoseptum (HM), or in between
586 somatic boundaries (central).

587

588 **Data analysis**

589 All the graphs were generated in the GraphPad Prism software. For quantifications,
590 standard error of the mean was calculated. To analyze significance between two samples, P
591 values were determined by performing the Mann-Whitney *U* test.

ACKNOWLEDGEMENTS

We thank the zebrafish community for providing probes and reagents; Holger Knaut for BAC clones; Jason Berman for *UAS:NTR-mCherry* fish; Sarah Childs and members of the Huang laboratory for discussion; and Paul Mains and James McGhee for critical comments on the manuscript.

COMPETING INTERESTS

The authors declare that no competing interests exist.

FUNDING

This study was supported by grants to P.H. from the Canadian Institute of Health Research (MOP-136926), Canada Foundation for Innovation John R. Evans Leaders Fund (Project 32920), and Startup Fund from the Alberta Children's Hospital Foundation. P.S. was supported by the Eyes High Postdoctoral Fellowship. T.D.R. was supported by the Queen Elizabeth Scholarship.

FIGURE LEGENDS

Figure 1. The dermomyotome is marked by the expression of ECM genes. (A) Double fluorescent in situ hybridization showed the co-expression of ECM genes *col1a2*, *col5a1*, and *cilp* (red) with the muscle progenitor cell marker *pax7* (green) in the dermomyotome (arrows) at 3 dpf. Both lateral and transverse views are shown. Note that high-level *col1a2* expression in skin cells bleeds into the red channel (arrowheads). (B) Schematics of the *col1a2:Gal4* BAC reporter. (C) *col1a2*$^{NTR\text{-}mCherry}$*; α-actin:GFP* fish at 3 dpf showed mCherry expression (red) in the dermomyotome (short arrows) on the surface of muscles, labeled by *α-actin:GFP* (green), cells around the notochord (arrowheads), and occasionally muscle fibers (long arrows). (D) *col1a2*$^{NTR\text{-}mCherry}$ fish were stained with the anti-Pax7 antibody at 2 dpf. Most *mCherry*$^{+}$ dermomyotome cells (red, arrows in expanded views) are co-labeled with Pax7 (weaker staining). Note that Pax7 also labels *mCherry*$^{-}$ xanthophores (bean-shaped nuclei with stronger Pax7 staining, arrowheads). (E) Transverse views of *col1a2*$^{NTR\text{-}mCherry}$ fish at 22 mm SL. Expanded views of the boxed region are shown on the right. mCherry expression (red) can be observed in the presumptive dermomyotome (short arrows), the skin (long arrows), scales (arrowheads), and occasionally muscles (asterisks). The autofluorescence signal (green) is shown to highlight the outline of muscle fibers. Scale bars: 50 μm, except 200 μm in the full view of (E).

Figure 2. Characterization of *col1a2*$^{+}$ dermomyotome. (A) Quantification of dermomyotome cells per somite in *col1a2*$^{NTR\text{-}mCherry}$ fish stained with anti-Pax7 antibody at 2 dpf. (B) Schematics of dermomyotome cell distribution. (C) Distribution of Pax7^{+}Col1a2^{+} dermomyotome cells based on their locations. (D) Mosaic *col1a2*^{Kaede} embryos were selected to image single dermomyotome cells. Examples of dermomyotome cells in between vertical myosepta (VM) and along the VM are shown. Dermomyotome cells display ramified morphology with lamelipodia-like structures (arrows) and fine cellular protrusions (arrowheads in expanded views). (E) *col1a2:Gal4; UAS:NTR-mCherry; UAS:Kaede* embryos were imaged at 2 dpf for 7.9 hours. Snapshots from Movie 1 show the division of a dermomyotome cell (arrows). Scale bars: 50 μm, except 20 μm in expanded views in (D).

Figure 3. *col1a2*$^{+}$ dermomyotome cells contribute to normal muscle growth. (A) Schematics of photoconversion-based lineage tracing. (B) *col1a2*^{Kaede} embryos were photoconverted at 3 dpf, and imaged at indicated time points. Color coded depth projections (green corresponds to superficial slices, while red denotes deep slices) of converted *Kaede*^{red} showed that new *Kaede*^{red} muscle fibers (arrow) emerged at 48-hour post conversion. An existing muscle fiber through all 3 time points is indicated by arrowheads. (C) Schematics of Cre-mediated lineage tracing experiments. (D) *col1a2*$^{Cre-ERT2}$*; ubi:Switch* embryos were pulsed with 4-OHT for 2 hours at 3 dpf to induce EGFP excision, and imaged for 4 days. Color coded depth projections of the mCherry expression are shown. "Switched" *mCherry*$^{+}$ dermomyotome cells (arrowheads) at the "+24 hr" time point generated new *mCherry*$^{+}$ muscle fibers (arrows) starting from the "+48 hr" time point. Scale bars: 50 μm.

Figure 4. ECM dynamics during muscle injury repair. (A) *col1a2*$^{NTR-mCherry}$*; α-actin:GFP* embryos were needle injured at 3 dpf, and imaged at 1, 24, 48, and 72 hpi. Injured muscles (asterisks) can be identified by the lack of *α-actin:GFP* expression (green), while regenerated muscles were marked by elevated *α-actin:GFP* expression. *mCherry*$^{+}$ dermomyotome cells (arrows) emerged at the site of injury at 24 hpi, and generated new *mCherry*$^{+}$ muscle fibers by 72 hpi. (B) Wild-type embryos were needle stabbed to injure muscles near the end of yolk extension (asterisks) at 3 dpf, fixed at different time points, and stained with the stem cell marker (*pax7*), muscle markers (*myoD* and *myogenin*), and ECM markers (*col1a2* and *col5a1*). All markers showed upregulation at the site of injury starting from 24 hpi (arrows). Scale bars: 50 μm.

Figure 5. Single cell clonal analysis of dermomyotome cells. (A) Schematics of single cell lineage tracing experiments. Isolated *Kaede*^{green} dermomyotome cells in *col1a2*^{Kaede} fish at 3 dpf were photoconverted to *Kaede*^{red}. Immediately after the photoconversion, muscles near the converted *Kaede*^{red} cell were damaged by laser ablation (asterisk). The lineage of the *Kaede*^{red} cell was inferred by imaging the same region every 24 hours. (B) Single cell lineage tracing in *col1a2*^{Kaede} embryos. Four types of responses are represented in cartoons on top with corresponding examples shown at the bottom. Each embryo was imaged at 3 dpf immediately after the photoconversion but before the injury and then at 1, 24, 48, 72 hpi.

669 Note that laser ablation often resulted in elevated autofluorescence at the center of the injury
670 (asterisks). Individual dermomyotome cells and their descendants are marked with cyan dots.
671 The nuclei of newly formed muscle fibers can be identified by high level of *Kaede*^{red}
672 expression (arrows). (C) Quantification of response types of dermomyotome cells. (D)
673 Quantification of cell distance from the injury site in different response types. Each point
674 represents one dermomyotome cell under injured condition (68 cells in total). Type I/II (empty
675 dots) and III/IV (solid dots) responses represent quiescent and activated cells, respectively.
676 Data are plotted with mean ± SEM. Statistics: Mann-Whitney *U* test. NS: not significant. (E)
677 Quantification of response types of dermomyotome cells with respect to their initial locations.
678 Cells near myosepta (n=23) are more likely to generate type III/IV responses compared to
679 cells in between myosepta (n=45). Scale bar: 50 μm.
680
681 **Figure 6. *In vivo* dynamics of dermomyotome cells.** (A) Schematic representation of the
682 experiment in (B). *col1a2*^{Kaede} embryos were needle injured, photoconverted at 59 hpf, and
683 then imaged from 0 to 23 hpi. (B) Representative snapshots from Movie 3 show the dynamics
684 of 2 photoconverted *Kaede*^{red} cells during first 23 hours of regeneration. Both cells were
685 within the muscle injury area, which spanned two somites (outlined by dash lines). Cell “a”
686 (white arrows) maintained the ramified morphology, and divided once at 7 hpi generating two
687 daughter cells with similar morphologies. By contrast, cell “b” (yellow arrows) extended to
688 form an elongated morphology (arrowheads), and divided once at 16 hpi generating two
689 polarized daughter cells. (C) Schematic representation of the experiment in (D). Mosaic
690 *col1a2*^{Kaede} embryos were injured at 3 dpf, and imaged from 29 to 48 hpi. (D) A *Kaede*$^{+}$
691 dermomyotome cell (arrows) near the injury site (asterisks) elongated at 34 hpi (white
692 arrowheads), formed protrusions at 39 hpi, and fused with a neighboring muscle fiber at 40
693 hpi. The newly formed muscle fiber can be visualized by the weak Kaede expression
694 throughout the muscle fiber and the strong Kaede expression in the nucleus (yellow
695 arrowheads). Scale bars: 50 μm.
696
697 **Figure 7. *col1a2*$^{+}$ dermomyotome cells generate new muscle fibers primarily by cell**
698 **fusion.** (A) Schematics of lineage tracing experiments. *co1a2*$^{Cre\text{-}ERT2}$*; ubi:Switch* embryos
699 treated with 4-OHT for 3.5 hours at 3 dpf were either needle injured or left uninjured (controls)

and imaged 75 hours after the 4-OHT treatment. (B) Two possible modes of new muscle fiber formation. Cell fusion would generate an *mCherry*$^{+}$*EGFP*$^{+}$ fiber (yellow), whereas *de novo* fiber formation would result in an *mCherry*$^{+}$*EGFP*$^{-}$ fiber (red). (C) Quantification of two modes of new fiber formation in control and injured embryos. (D) In control embryos, new muscle fibers were formed primarily through cell fusion (arrows), whereas in injured embryos, new fibers were generated by both fusion (arrows) and occasionally *de novo* fiber formation (arrowheads). (E) Schematics of dermomyotome ablation experiment. (F) *col1a2*$^{NTR\text{-mCherry}}$ or control embryos treated with MTZ at 2-3 dpf were injured at 3 dpf and stained for *myoD* expression at 24 hpi. All control embryos (38/38) displayed significant *myoD* upregulation (arrow), while most ablated embryos (68/88) showed no specific *myoD* induction at the injury site (asterisk). (G) Model of muscle injury repair by dermomyotome cells. Upon muscle injury (1), activated dermomyotome cells transform from the ramified morphology to a highly polarized morphology extending long cellular projections along muscle fibers (2). The activated cell proliferates to generate more elongated daughter cells (3), some of which fuse with an existing muscle fiber to regenerate the damaged region (4). Scale bars: 50 μm.

715 **SUPPLEMENTARY INFORMATION**

716

717 **Figure S1. Validation of the *col1a2*^{Kaede} line**. Double fluorescent in situ hybridization using
718 *kaede* and *col1a2* probes were performed in *col1a2*^{Kaede} embryos at 3 dpf. Co-expression of
719 *kaede* (green) and the endogenous *col1a2* (red) can be observed in dermomyotome cells
720 (white arrows), tenocytes along the vertical myoseptum (yellow arrows), and deep interstitial
721 cells around the notochord (cyan arrows). Note that *col1a2*^{Kaede} was not expressed in the skin
722 cells (arrowheads) as *col1a2*. Scale bar: 50 μm.

723

724 **Figure S2. ECM molecules are upregulated during muscle injury repair.** Wild-type
725 embryos were needle stabbed to injure a somite near the end of yolk extension (asterisks) at
726 3dpf, and fixed at 7, 24, 48, and 76 hpi. Embryos were then stained with ECM markers
727 (*col1a1a*, *cilp*, *postnb*, and *sparc*). All markers showed upregulation at the site of injury
728 starting from 24 hpi (arrows). Scale bars: 50 μm.

729

730 **Figure S3. Kaede protein is preferentially localized in nuclei of muscle fibers.** (A) Wild-
731 type embryos were injected with Kaede mRNA, and imaged at 66 hpf. Kaede protein (green)
732 is preferentially localized in the nuclei of muscle fibers (arrow). (B) *col1a2*^{Kaede} embryos were
733 injured at 3 dpf, and stained at 48 hpi with the anti-Pax7 antibody (green). *Kaede*$^{+}$
734 dermomyotome derived cells (red) contributed to muscle injury repair (boxed regions). The
735 expanded views show that newly formed muscle fiber displayed strong Kaede expression in
736 the nucleus (arrows), which was not labelled by Pax7. By contrast, a small elongated *Kaede*$^{+}$
737 cell between muscle fibers was Pax7 positive (arrowheads). (C) Quantification of clone size
738 in single cell clonal analysis described in Fig 5. Dermomyotome cells under the injury
739 condition (blue, n=68) tend to generate larger clones compared to cells in the wild-type
740 condition (green, n=65). Scale bars: 50 μm.

741

742 **Movie 1. Expression pattern of the *col1a2* transgenic line.** A confocal z-stack of
743 *col1a2:Gal4; UAS:NTR-mCherry; α-actin:GFP* embryos at 3 dpf shows mCherry expression
744 (green) in dermomyotome cells, some muscle fibers, tenocytes and notochord-associated
745 cells (arrows). Muscle fibers are labeled with *α-actin:GFP* (magenta). Scale bar: 50 μm.

Movie 2. Dynamics *col1a2*$^{+}$ dermomyotome cells in quiescent state. *col1a2:Gal4; UAS:NTR-mCherry; UAS:Kaede* embryos were imaged at 2 dpf for 7.9 hours. *col1a2*$^{+}$ dermomyotome cells cover the entire surface of a somite. When a dermomyotome cell divides, daughter cells reclaim the same surface area soon after division. Five different cell divisions are indicated by arrows. Scale bars: 50 μm.

Movie 3. Dynamics *col1a2*$^{+}$ dermomyotome cells in injured condition. *col1a2*^{Kaede} embryos were injured, photoconverted at 59 hpf, and then imaged over 23 hours (0-23 hpi). Cells “a” and “b” were within the injured area while the cell “c” was in the uninjured area. Cell “a” (white arrows) maintained the ramified morphology, and divided once at 7 hpi generating two daughter cells with similar morphologies. By contrast, cell “b” (yellow arrows) extended to form an elongated morphology (arrowheads), and divided once at 16 hpi generating two polarized daughter cells. Cell “c” (cyan arrows) did not divide and remained its ramified morphology. Scale bars: 50 μm.

Movie 4. Generation of new muscle fibers by cell fusion. *col1a2*^{Kaede} fish was injured at 3 dpf and imaged from 29 hpi onwards. A *Kaede*$^{+}$ dermomyotome cell (arrows) near the injury site elongated at 34 hpi (white arrowheads), formed protrusions at 39 hpi, and fused with a neighboring muscle fiber at 40 hpi. The newly formed muscle fiber can be identified by the weak Kaede expression throughout the muscle fiber and the strong Kaede expression in the nucleus (yellow arrowheads). Scale bars: 50 μm.

REFERENCES

Akitake, C. M., Macurak, M., Halpern, M. E. and Goll, M. G. (2011). Transgenerational analysis of transcriptional silencing in zebrafish. *Dev Biol* **352**, 191-201.

Ando, R., Hama, H., Yamamoto-Hino, M., Mizuno, H. and Miyawaki, A. (2002). An optical marker based on the UV-induced green-to-red photoconversion of a fluorescent protein. *Proc Natl Acad Sci U S A* **99**, 12651-12656.

Baghdadi, M. B., Castel, D., Machado, L., Fukada, S. I., Birk, D. E., Relaix, F., Tajbakhsh, S. and Mourikis, P. (2018). Reciprocal signalling by Notch-Collagen V-CALCR retains muscle stem cells in their niche. *Nature* **557**, 714-718.

Bentzinger, C. F., von Maltzahn, J., Dumont, N. A., Stark, D. A., Wang, Y. X., Nhan, K., Frenette, J., Cornelison, D. D. and Rudnicki, M. A. (2014). Wnt7a stimulates myogenic stem cell motility and engraftment resulting in improved muscle strength. *J Cell Biol* **205**, 97-111.

Bentzinger, C. F., Wang, Y. X., Dumont, N. A. and Rudnicki, M. A. (2013a). Cellular dynamics in the muscle satellite cell niche. *EMBO Rep* **14**, 1062-1072.

Bentzinger, C. F., Wang, Y. X., von Maltzahn, J., Soleimani, V. D., Yin, H. and Rudnicki, M. A. (2013b). Fibronectin regulates Wnt7a signaling and satellite cell expansion. *Cell Stem Cell* **12**, 75-87.

Bussmann, J. and Schulte-Merker, S. (2011). Rapid BAC selection for tol2-mediated transgenesis in zebrafish. *Development* **138**, 4327-4332.

Christ, B. and Scaal, M. (2008). Formation and differentiation of avian somite derivatives. *Adv Exp Med Biol* **638**, 1-41.

Curado, S., Stainier, D. Y. and Anderson, R. M. (2008). Nitroreductase-mediated cell/tissue ablation in zebrafish: a spatially and temporally controlled ablation method with applications in developmental and regeneration studies. *Nat Protoc* **3**, 948-954.

Davison, J. M., Akitake, C. M., Goll, M. G., Rhee, J. M., Gosse, N., Baier, H., Halpern, M. E., Leach, S. D. and Parsons, M. J. (2007). Transactivation from Gal4-VP16 transgenic insertions for tissue-specific cell labeling and ablation in zebrafish. *Dev Biol* **304**, 811-824.

Devoto, S. H., Stoiber, W., Hammond, C. L., Steinbacher, P., Haslett, J. R., Barresi, M. J., Patterson, S. E., Adiarte, E. G. and Hughes, S. M. (2006). Generality of vertebrate developmental patterns: evidence for a dermomyotome in fish. *Evol Dev* **8**, 101-110.

Dumont, N. A., Bentzinger, C. F., Sincennes, M. C. and Rudnicki, M. A. (2015). Satellite Cells and Skeletal Muscle Regeneration. *Compr Physiol* **5**, 1027-1059.

El Fahime, E., Torrente, Y., Caron, N. J., Bresolin, M. D. and Tremblay, J. P. (2000). In vivo migration of transplanted myoblasts requires matrix metalloproteinase activity. *Exp Cell Res* **258**, 279-287.

Feng, X., Adiarte, E. G. and Devoto, S. H. (2006). Hedgehog acts directly on the zebrafish dermomyotome to promote myogenic differentiation. *Dev Biol* **300**, 736-746.

Fry, C. S., Kirby, T. J., Kosmac, K., McCarthy, J. J. and Peterson, C. A. (2017). Myogenic Progenitor Cells Control Extracellular Matrix Production by Fibroblasts during Skeletal Muscle Hypertrophy. *Cell Stem Cell* **20**, 56-69.

Gros, J., Manceau, M., Thomé, V. and Marcelle, C. (2005). A common somitic origin for embryonic muscle progenitors and satellite cells. *Nature* **435**, 954-958.

Grueber, W. B. and Sagasti, A. (2010). Self-avoidance and tiling: Mechanisms of dendrite and axon spacing. *Cold Spring Harb Perspect Biol* **2**, a001750.

Gurevich, D. B., Nguyen, P. D., Siegel, A. L., Ehrlich, O. V., Sonntag, C., Phan, J. M., Berger, S., Ratnayake, D., Hersey, L., Berger, J., et al. (2016). Asymmetric division of clonal muscle stem cells coordinates muscle regeneration in vivo. *Science* **353**, aad9969.

Hammond, C. L., Hinits, Y., Osborn, D. P., Minchin, J. E., Tettamanti, G. and Hughes, S. M. (2007). Signals and myogenic regulatory factors restrict pax3 and pax7 expression to dermomyotome-like tissue in zebrafish. *Dev Biol* **302**, 504-521.

Higashijima, S., Okamoto, H., Ueno, N., Hotta, Y. and Eguchi, G. (1997). High-frequency generation of transgenic zebrafish which reliably express GFP in whole muscles or the whole body by using promoters of zebrafish origin. *Dev Biol* **192**, 289-299.

Hollway, G. E., Bryson-Richardson, R. J., Berger, S., Cole, N. J., Hall, T. E. and Currie, P. D. (2007). Whole-somite rotation generates muscle progenitor cell compartments in the developing zebrafish embryo. *Dev Cell* **12**, 207-219.

Jockusch, H. and Voigt, S. (2003). Migration of adult myogenic precursor cells as revealed by GFP/nLacZ labelling of mouse transplantation chimeras. *J Cell Sci* **116**, 1611-1616.

Kassar-Duchossoy, L., Giacone, E., Gayraud-Morel, B., Jory, A., Gomès, D. and Tajbakhsh, S. (2005). Pax3/Pax7 mark a novel population of primitive myogenic cells during development. *Genes Dev* **19**, 1426-1431.

Kimmel, C. B., Ballard, W. W., Kimmel, S. R., Ullmann, B. and Schilling, T. F. (1995). Stages of embryonic development of the zebrafish. *Dev Dyn* **203**, 253-310.

Knappe, S., Zammit, P. S. and Knight, R. D. (2015). A population of Pax7-expressing muscle progenitor cells show differential responses to muscle injury dependent on developmental stage and injury extent. *Front Aging Neurosci* **7**, 161.

Kuang, S., Kuroda, K., Le Grand, F. and Rudnicki, M. A. (2007). Asymmetric self-renewal and commitment of satellite stem cells in muscle. *Cell* **129**, 999-1010.

Le Guellec, D., Morvan-Dubois, G. and Sire, J. Y. (2004). Skin development in bony fish with particular emphasis on collagen deposition in the dermis of the zebrafish (Danio rerio). *Int J Dev Biol* **48**, 217-231.

Lepper, C., Partridge, T. A. and Fan, C. M. (2011). An absolute requirement for Pax7-positive satellite cells in acute injury-induced skeletal muscle regeneration. *Development* **138**, 3639-3646.

Liu, N., Garry, G. A., Li, S., Bezprozvannaya, S., Sanchez-Ortiz, E., Chen, B., Shelton, J. M., Jaichander, P., Bassel-Duby, R. and Olson, E. N. (2017). A Twist2-dependent progenitor cell contributes to adult skeletal muscle. *Nat Cell Biol* **19**, 202-213.

Love, N. R., Chen, Y., Ishibashi, S., Kritsiligkou, P., Lea, R., Koh, Y., Gallop, J. L., Dorey, K. and Amaya, E. (2013). Amputation-induced reactive oxygen species are required for successful Xenopus tadpole tail regeneration. *Nat Cell Biol* **15**, 222-228.

Mosimann, C., Kaufman, C. K., Li, P., Pugach, E. K., Tamplin, O. J. and Zon, L. I. (2011). Ubiquitous transgene expression and Cre-based recombination driven by the ubiquitin promoter in zebrafish. *Development* **138**, 169-177.

Murphy, M. M., Lawson, J. A., Mathew, S. J., Hutcheson, D. A. and Kardon, G. (2011). Satellite cells, connective tissue fibroblasts and their interactions are crucial for muscle regeneration. *Development* **138**, 3625-3637.

Nguyen, P. D., Gurevich, D. B., Sonntag, C., Hersey, L., Alaei, S., Nim, H. T., Siegel, A., Hall, T. E., Rossello, F. J., Boyd, S. E., et al. (2017). Muscle Stem Cells Undergo Extensive Clonal Drift during Tissue Growth via Meox1-Mediated Induction of G2 Cell-Cycle Arrest. *Cell Stem Cell* **21**, 107-119.e106.

Niethammer, P., Grabher, C., Look, A. T. and Mitchison, T. J. (2009). A tissue-scale gradient of hydrogen peroxide mediates rapid wound detection in zebrafish. *Nature* **459**, 996-999.

Pallafacchina, G., François, S., Regnault, B., Czarny, B., Dive, V., Cumano, A., Montarras, D. and Buckingham, M. (2010). An adult tissue-specific stem cell in its niche: a gene profiling analysis of in vivo quiescent and activated muscle satellite cells. *Stem Cell Res* **4**, 77-91.

Pipalia, T. G., Koth, J., Roy, S. D., Hammond, C. L., Kawakami, K. and Hughes, S. M. (2016). Cellular dynamics of regeneration reveals role of two distinct Pax7 stem cell populations in larval zebrafish muscle repair. *Dis Model Mech* **9**, 671-684.

Pisharath, H., Rhee, J. M., Swanson, M. A., Leach, S. D. and Parsons, M. J. (2007). Targeted ablation of beta cells in the embryonic zebrafish pancreas using E. coli nitroreductase. *Mech Dev* **124**, 218-229.

Ralliere, C., Fretaud, M., Thermes, V. and Rescan, P. Y. (2015). CILP1 is dynamically expressed in the developing musculoskeletal system of the trout. *Int J Dev Biol* **59**, 505-509.

Ratnayake, D. and Currie, P. D. (2017). Stem cell dynamics in muscle regeneration: Insights from live imaging in different animal models. *Bioessays* **39**.

Rayagiri, S. S., Ranaldi, D., Raven, A., Mohamad Azhar, N. I. F., Lefebvre, O., Zammit, P. S. and Borycki, A. G. (2018). Basal lamina remodeling at the skeletal muscle stem cell niche mediates stem cell self-renewal. *Nat Commun* **9**, 1075.

Relaix, F., Rocancourt, D., Mansouri, A. and Buckingham, M. (2005). A Pax3/Pax7-dependent population of skeletal muscle progenitor cells. *Nature* **435**, 948-953.

Rescan, P. Y., Ralliere, C., Chauvigné, F. and Cauty, C. (2005). Expression patterns of collagen I (alpha1) encoding gene and muscle-specific genes reveal that the lateral domain of the fish somite forms a connective tissue surrounding the myotome. *Dev Dyn* **233**, 605-611.

Roy, S. D., Williams, V. C., Pipalia, T. G., Li, K., Hammond, C. L., Knappe, S., Knight, R. D. and Hughes, S. M. (2017). Myotome adaptability confers developmental robustness to somitic myogenesis in response to fibre number alteration. *Dev Biol* **431**, 321-335.

Sacco, A., Doyonnas, R., Kraft, P., Vitorovic, S. and Blau, H. M. (2008). Self-renewal and expansion of single transplanted muscle stem cells. *Nature* **456**, 502-506.

Saclier, M., Yacoub-Youssef, H., Mackey, A. L., Arnold, L., Ardjoune, H., Magnan, M., Sailhan, F., Chelly, J., Pavlath, G. K., Mounier, R., et al. (2013). Differentially activated macrophages orchestrate myogenic precursor cell fate during human skeletal muscle regeneration. *Stem Cells* **31**, 384-396.

Saga, Y. and Takeda, H. (2001). The making of the somite: molecular events in vertebrate segmentation. *Nat Rev Genet* **2**, 835-845.

Sagar, Pröls, F., Wiegreffe, C. and Scaal, M. (2015). Communication between distant epithelial cells by filopodia-like protrusions during embryonic development. *Development* **142**, 665-671.

Sambasivan, R., Yao, R., Kissenpfennig, A., Van Wittenberghe, L., Paldi, A., Gayraud-Morel, B., Guenou, H., Malissen, B., Tajbakhsh, S. and Galy, A. (2011). Pax7-expressing satellite cells are indispensable for adult skeletal muscle regeneration. *Development* **138**, 3647-3656.

Scaal, M. and Christ, B. (2004). Formation and differentiation of the avian dermomyotome. *Anat Embryol (Berl)* **208**, 411-424.

Scharner, J. and Zammit, P. S. (2011). The muscle satellite cell at 50: the formative years. *Skelet Muscle* **1**, 28.

Schienda, J., Engleka, K. A., Jun, S., Hansen, M. S., Epstein, J. A., Tabin, C. J., Kunkel, L. M. and Kardon, G. (2006). Somitic origin of limb muscle satellite and side population cells. *Proc Natl Acad Sci U S A* **103**, 945-950.

Schindelin, J., Arganda-Carreras, I., Frise, E., Kaynig, V., Longair, M., Pietzsch, T., Preibisch, S., Rueden, C., Saalfeld, S., Schmid, B., et al. (2012). Fiji: an open-source platform for biological-image analysis. *Nat Methods* **9**, 676-682.

Scott, E. K., Mason, L., Arrenberg, A. B., Ziv, L., Gosse, N. J., Xiao, T., Chi, N. C., Asakawa, K., Kawakami, K. and Baier, H. (2007). Targeting neural circuitry in zebrafish using GAL4 enhancer trapping. *Nat Methods* **4**, 323-326.

Seger, C., Hargrave, M., Wang, X., Chai, R. J., Elworthy, S. and Ingham, P. W. (2011). Analysis of Pax7 expressing myogenic cells in zebrafish muscle development, injury, and models of disease. *Dev Dyn* **240**, 2440-2451.

Seo, H. C., Saetre, B. O., Håvik, B., Ellingsen, S. and Fjose, A. (1998). The zebrafish Pax3 and Pax7 homologues are highly conserved, encode multiple isoforms and show dynamic segment-like expression in the developing brain. *Mech Dev* **70**, 49-63.

Siegel, A. L., Atchison, K., Fisher, K. E., Davis, G. E. and Cornelison, D. D. (2009). 3D timelapse analysis of muscle satellite cell motility. *Stem Cells* **27**, 2527-2538.

Sire, J. Y. and Akimenko, M. A. (2004). Scale development in fish: a review, with description of sonic hedgehog (shh) expression in the zebrafish (Danio rerio). *Int J Dev Biol* **48**, 233-247.

Stellabotte, F. and Devoto, S. H. (2007). The teleost dermomyotome. *Dev Dyn* **236**, 2432-2443.

Stellabotte, F., Dobbs-McAuliffe, B., Fernández, D. A., Feng, X. and Devoto, S. H. (2007). Dynamic somite cell rearrangements lead to distinct waves of myotome growth. *Development* **134**, 1253-1257.

Thisse, B., Heyer, V., Lux, A., Alunni, V., Degrave, A., Seiliez, I., Kirchner, J., Parkhill, J. P. and Thisse, C. (2004). Spatial and temporal expression of the zebrafish genome by large-scale in situ hybridization screening. *Methods Cell Biol* **77**, 505-519.

Tierney, M. T., Gromova, A., Sesillo, F. B., Sala, D., Spenlé, C., Orend, G. and Sacco, A. (2016). Autonomous Extracellular Matrix Remodeling Controls a Progressive Adaptation in Muscle Stem Cell Regenerative Capacity during Development. *Cell Rep* **14**, 1940-1952.

Urciuolo, A., Quarta, M., Morbidoni, V., Gattazzo, F., Molon, S., Grumati, P., Montemurro, F., Tedesco, F. S., Blaauw, B., Cossu, G., et al. (2013). Collagen VI regulates satellite cell self-renewal and muscle regeneration. *Nat Commun* **4**, 1964.

949 **Webster, M. T., Manor, U., Lippincott-Schwartz, J. and Fan, C. M.** (2016). Intravital
950 Imaging Reveals Ghost Fibers as Architectural Units Guiding Myogenic Progenitors
951 during Regeneration. *Cell Stem Cell* **18**, 243-252.
952 **Westerfield, M.** (2000). *The Zebrafish Book: A Guide for the Laboratory Use of Zebrafish*
953 *(Danio Rerio)* (4 edn): University of Oregon.
954

Figure 1

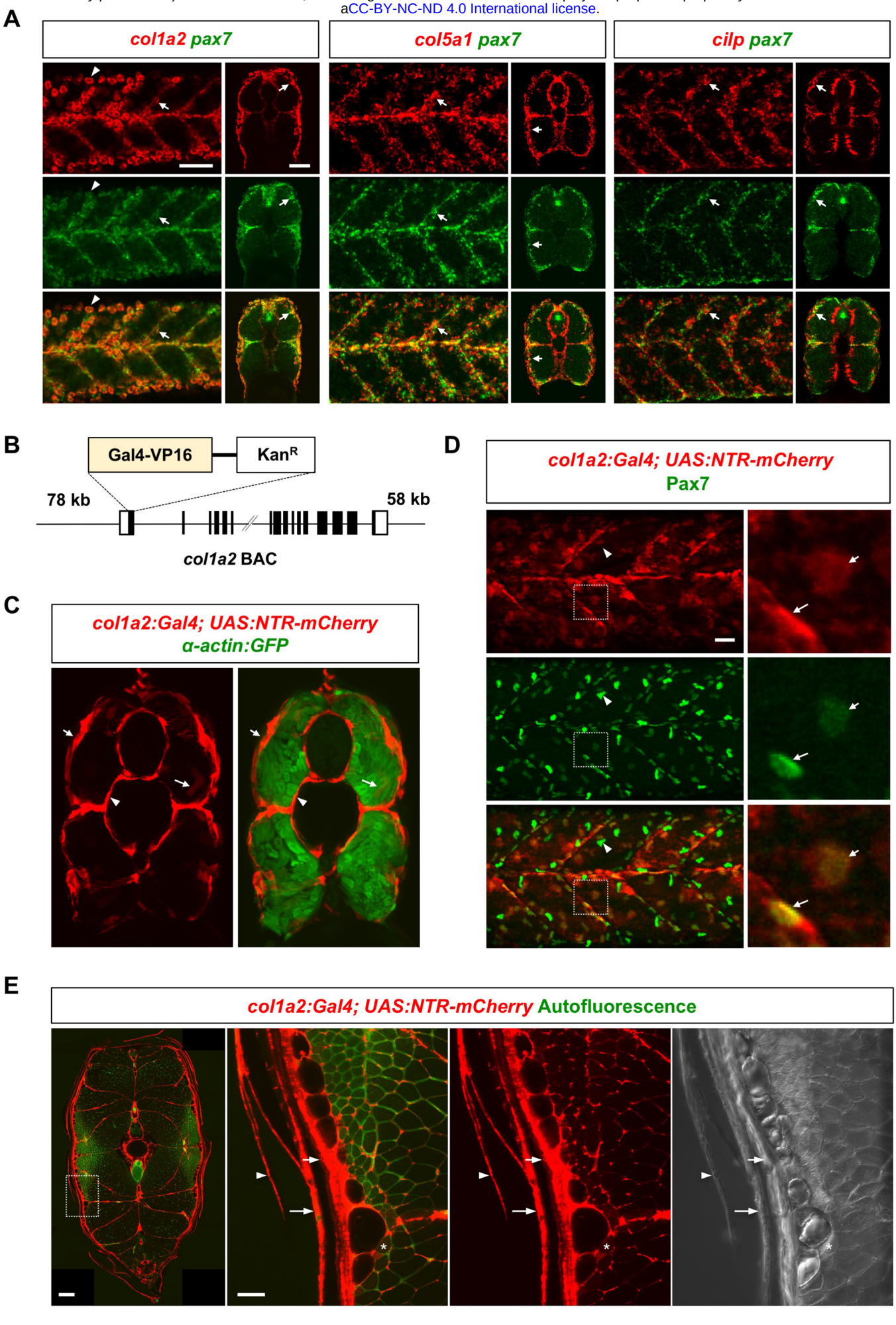

Figure 2

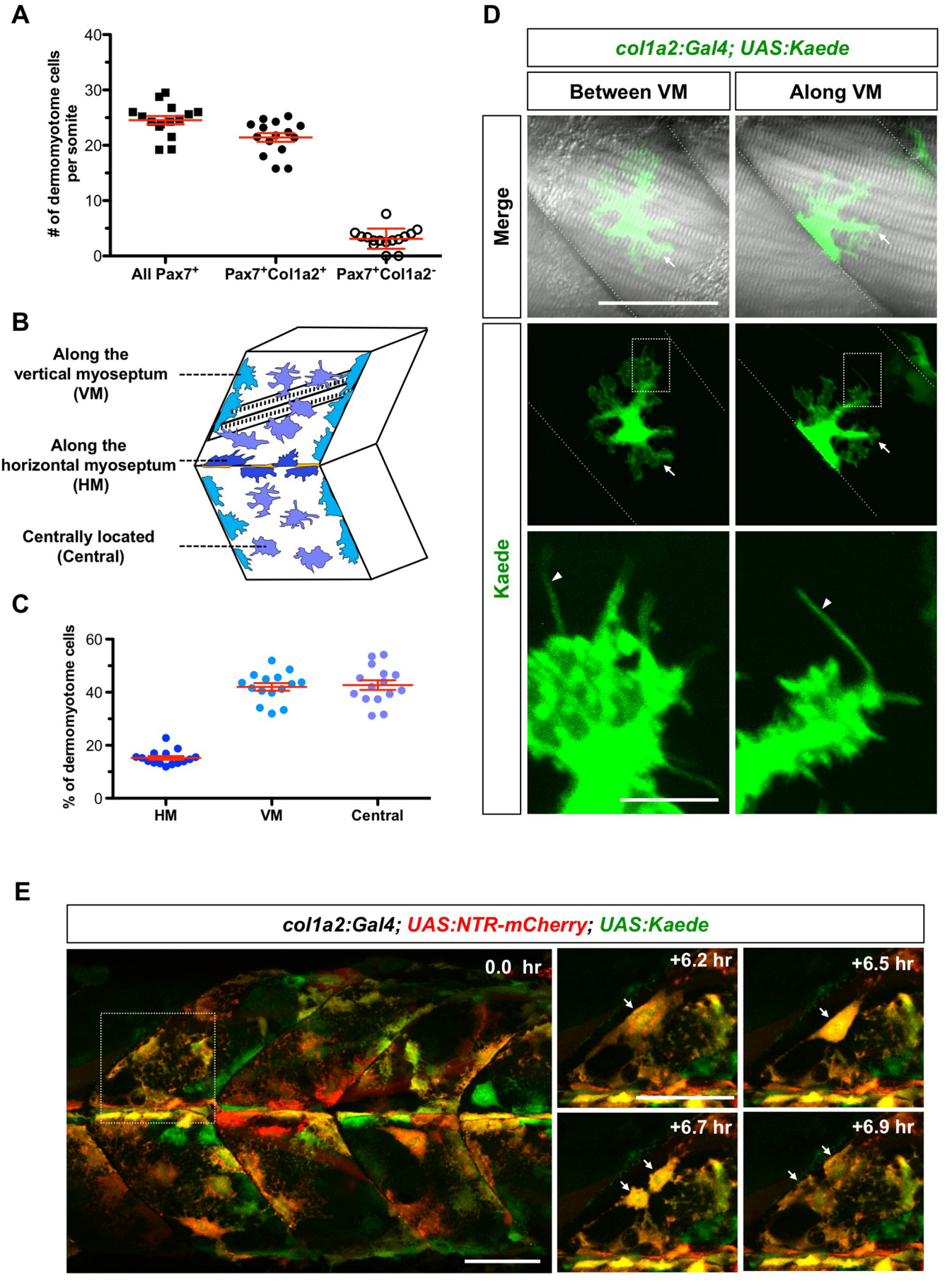

Figure 3

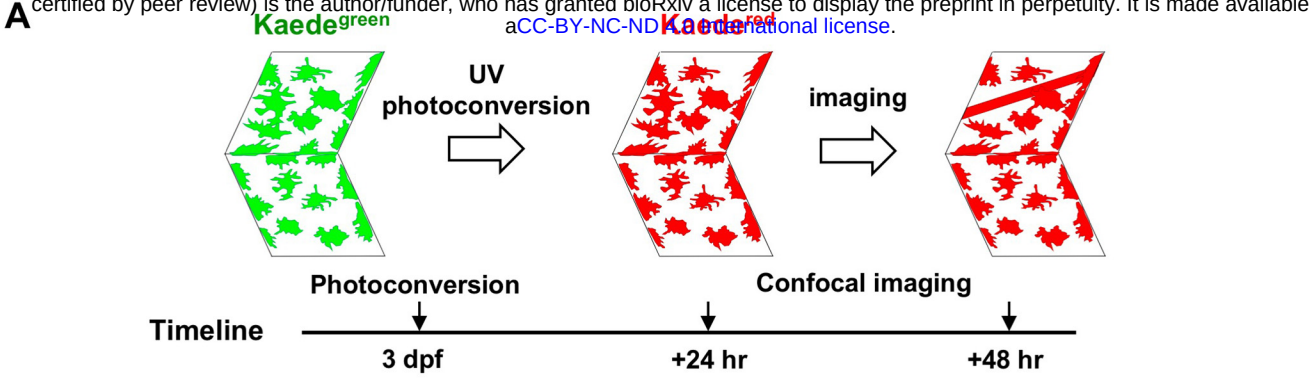

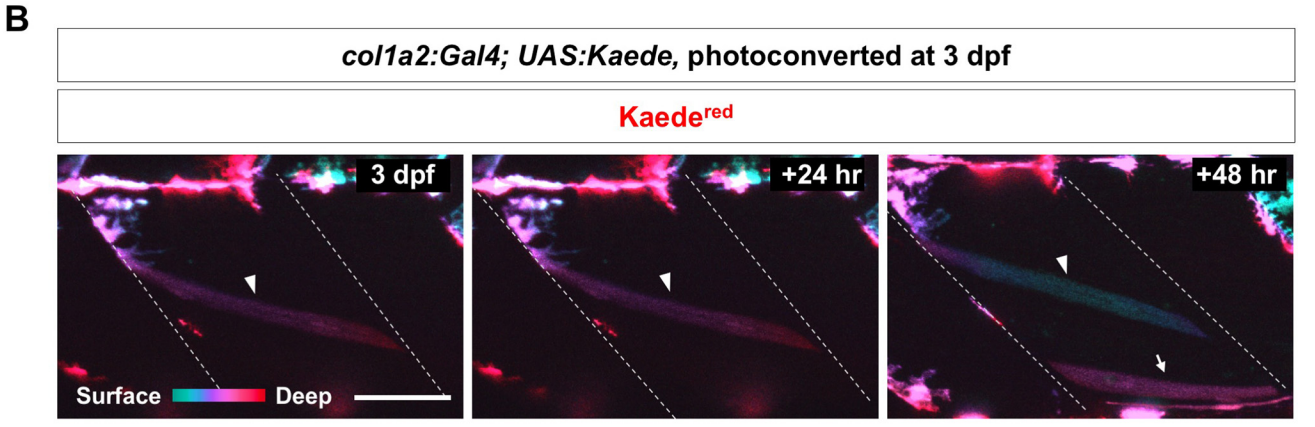

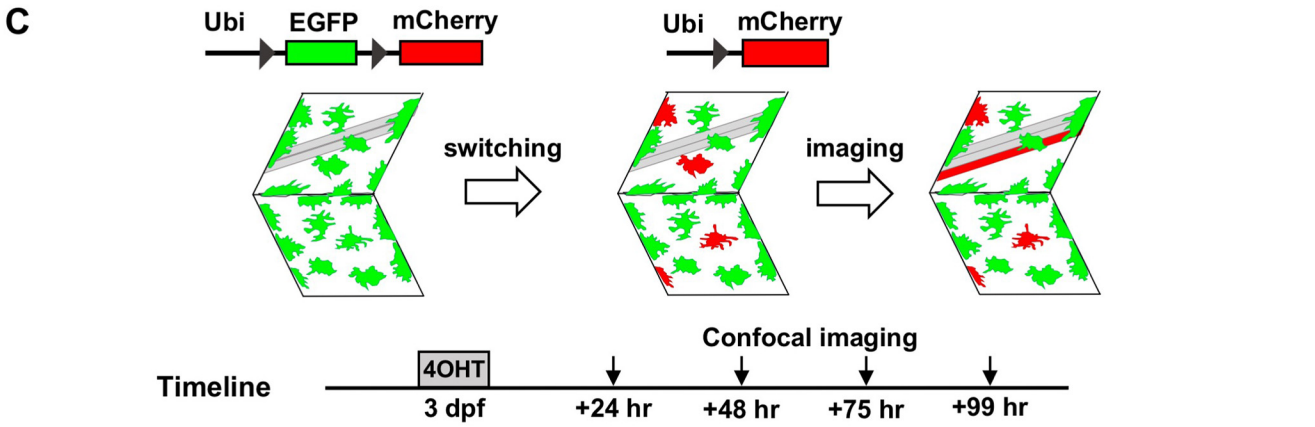

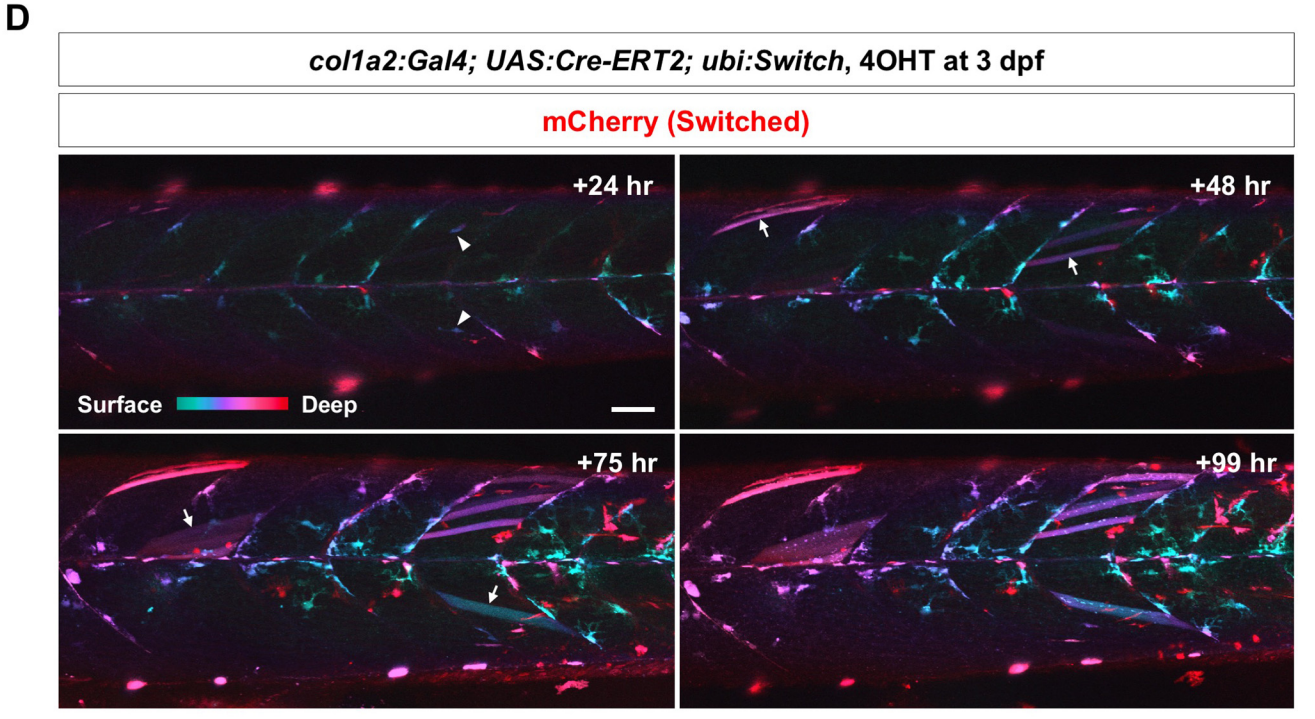

Figure 4

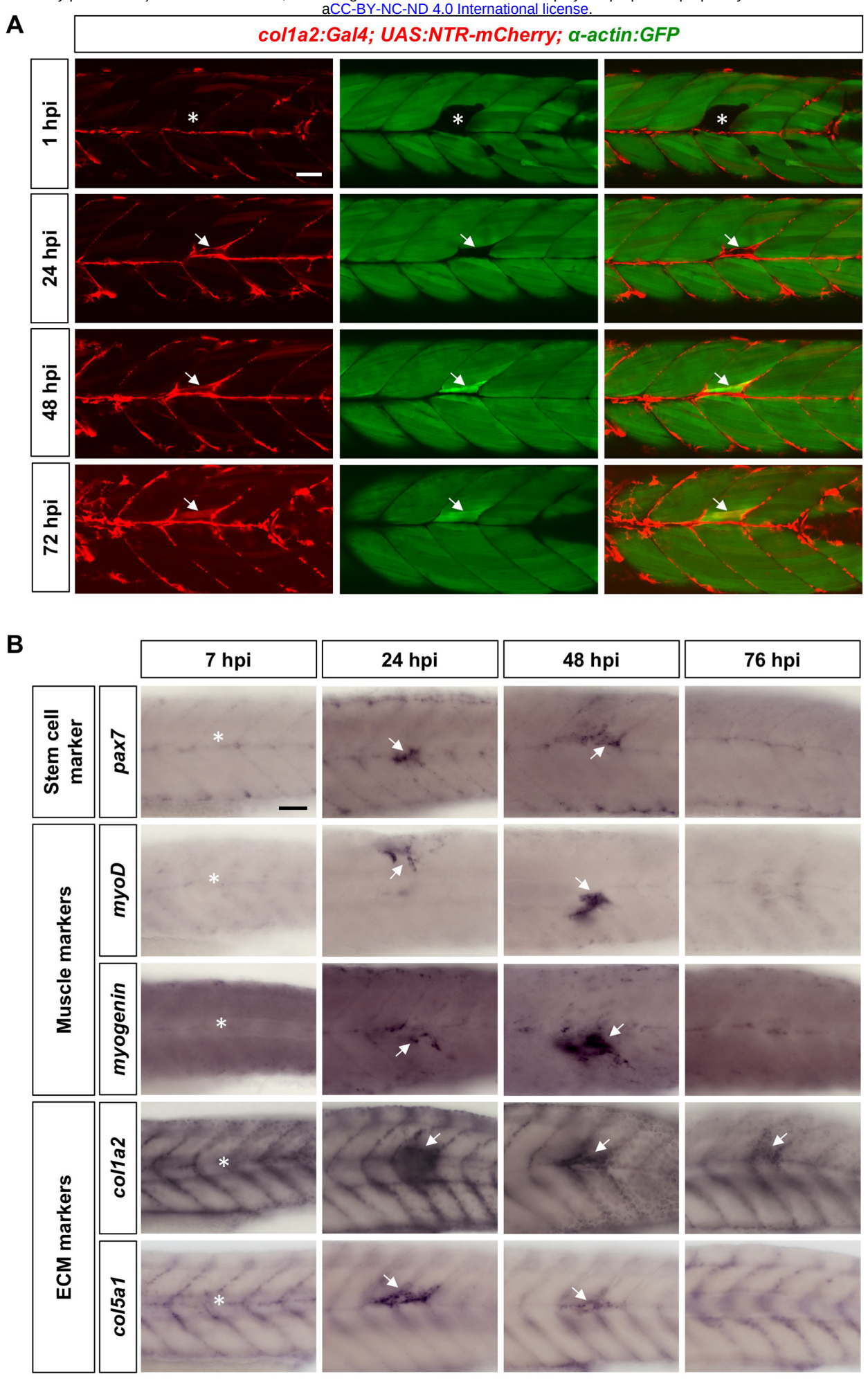

Figure 5

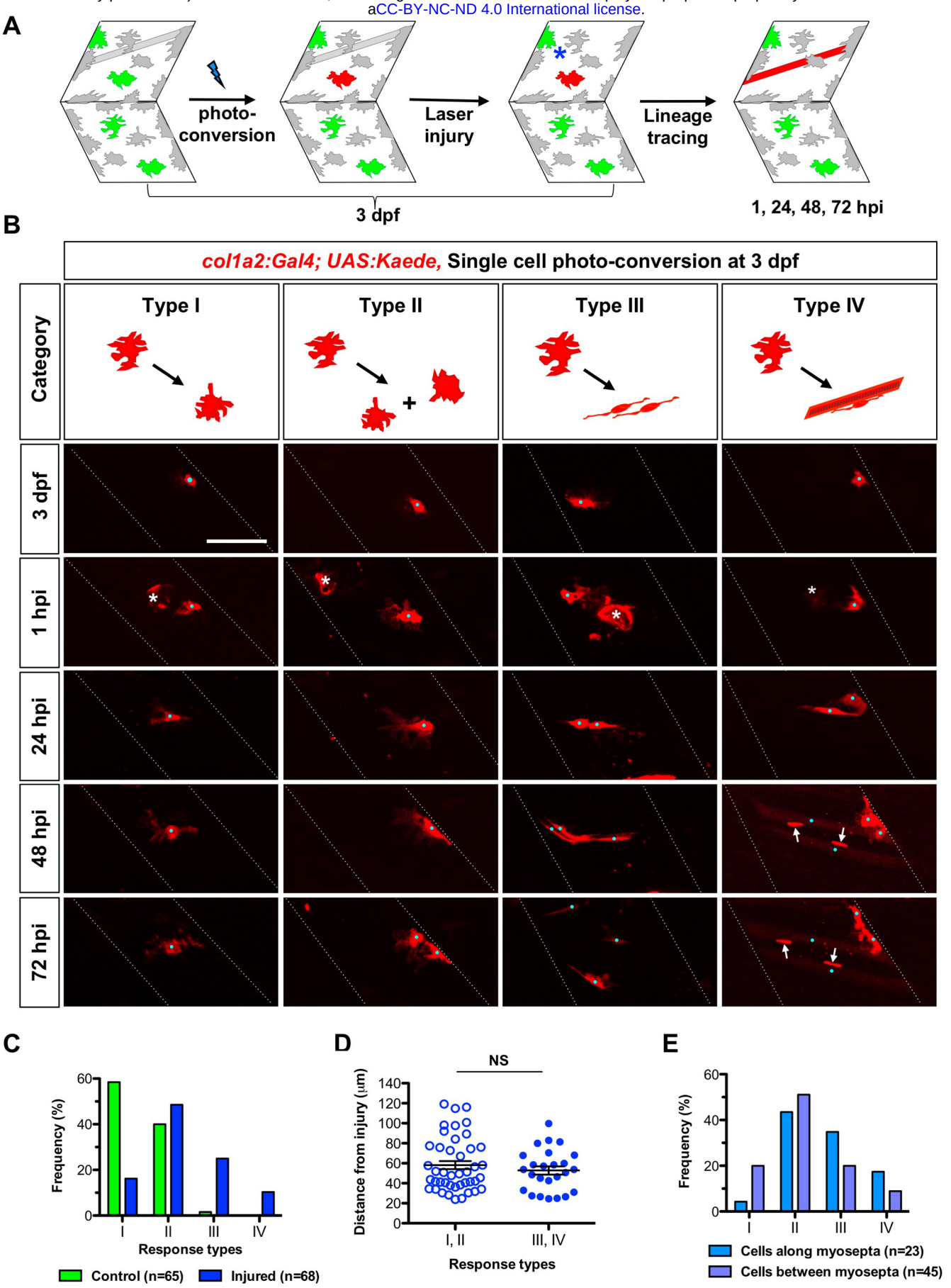

Figure 6

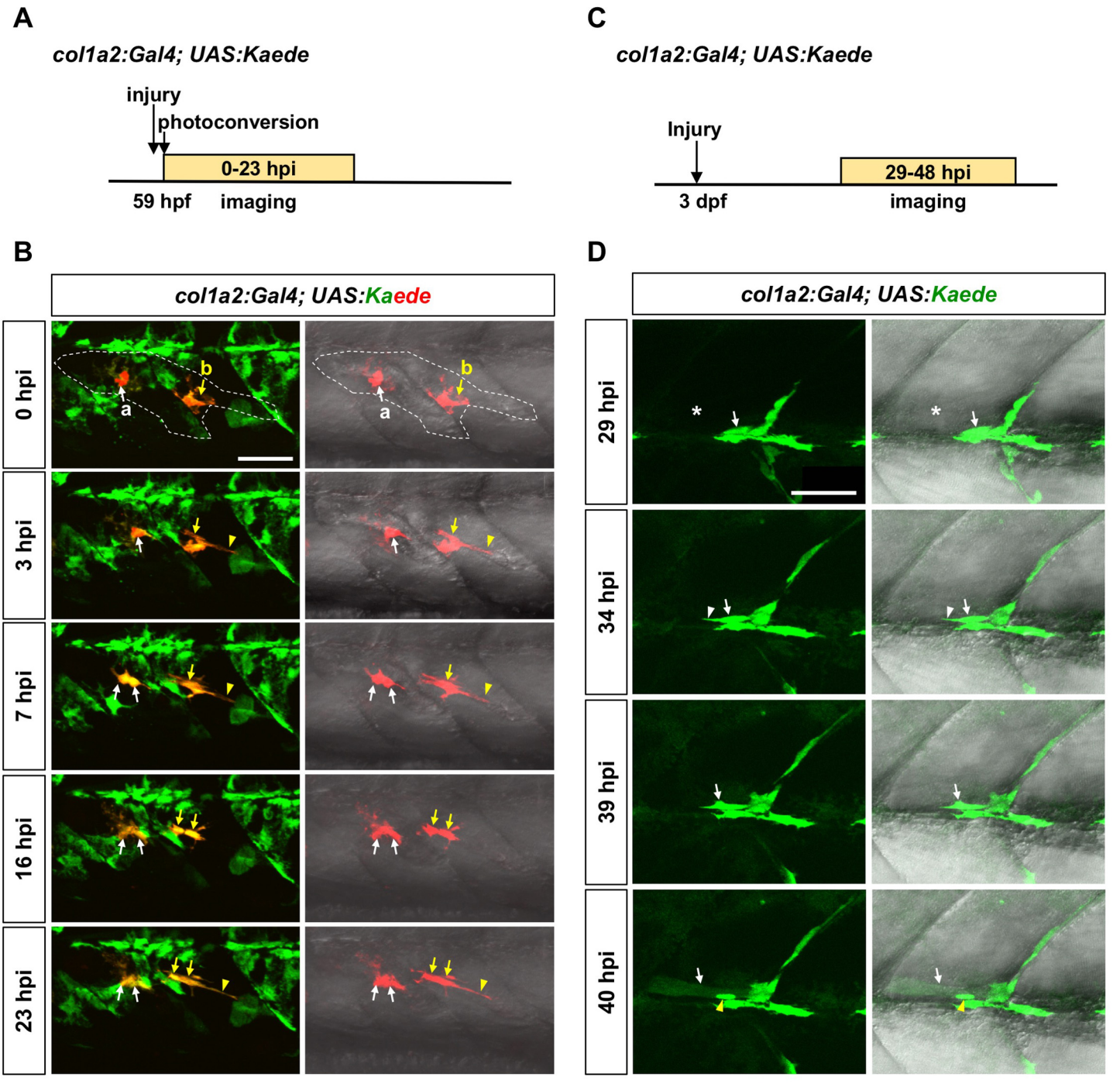

Figure 7

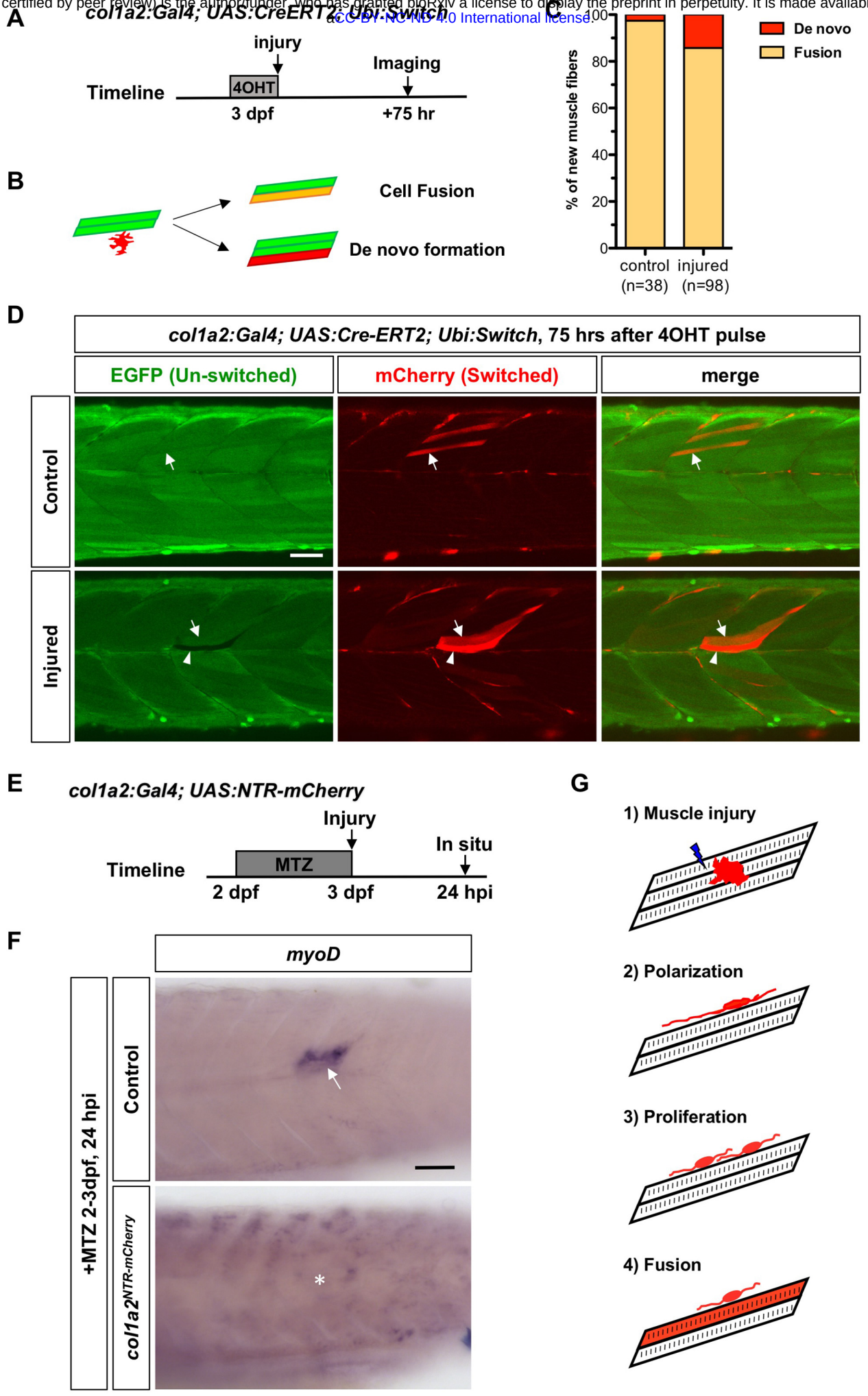

Figure S1

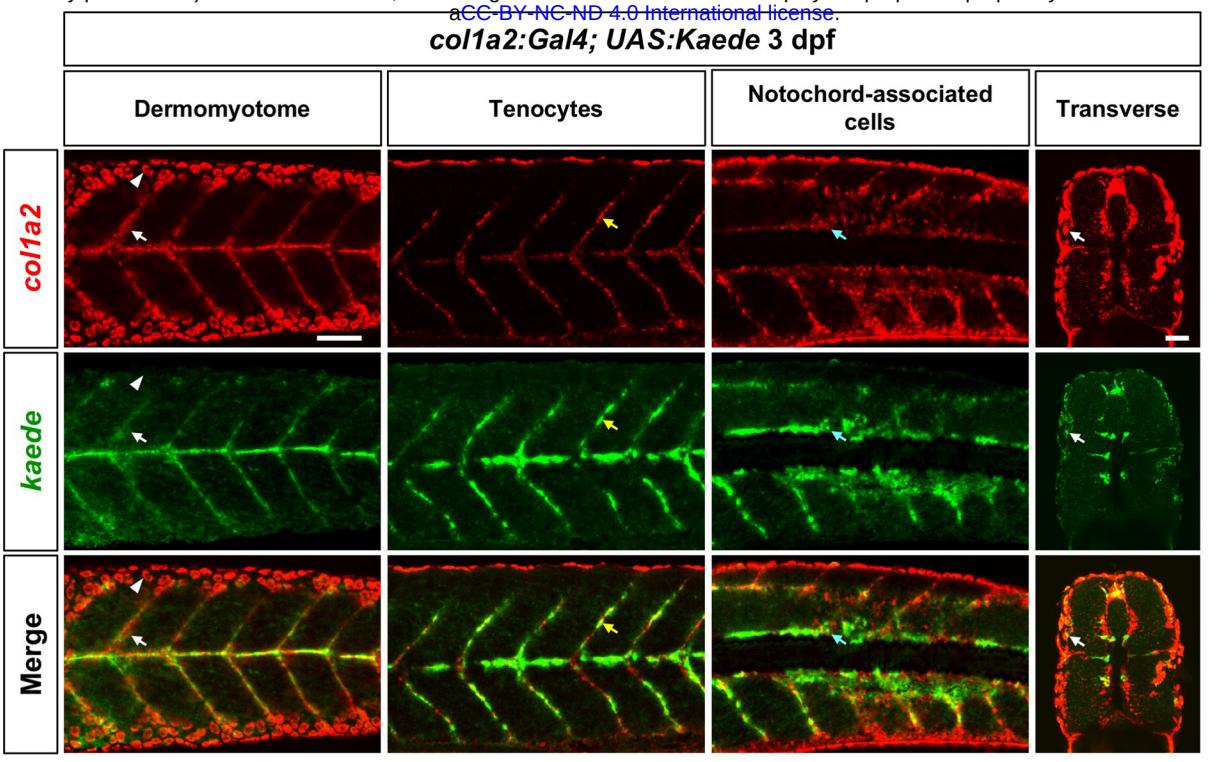

Figure S2

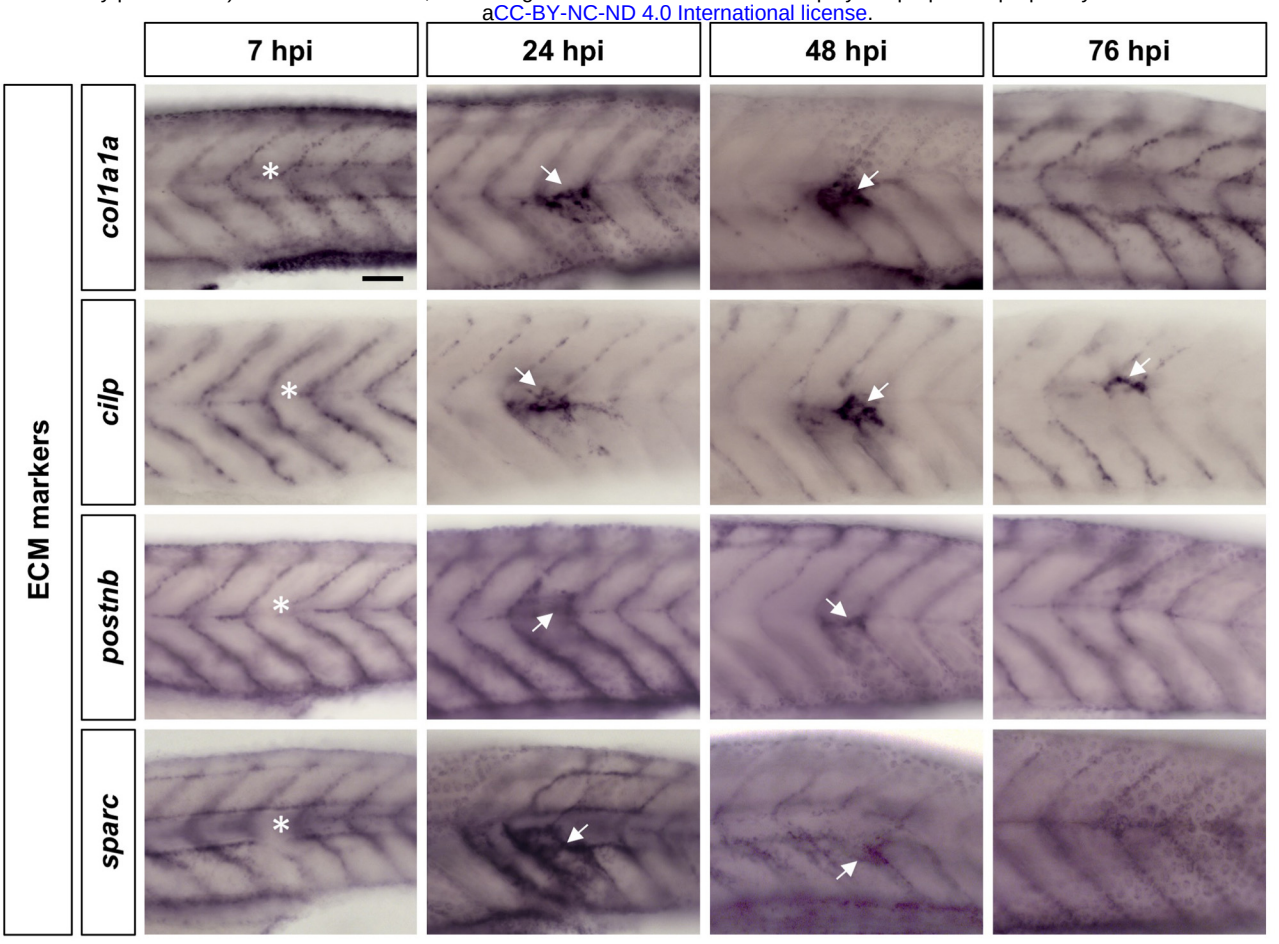

Figure S3